

Search for excited leptons in e^+e^- collisions at $\sqrt{s} = 189 - 209$ GeV

The DELPHI Collaboration

Abstract

A search for excited lepton production in e^+e^- collisions was performed using the data collected by the DELPHI detector at LEP at centre-of-mass energies ranging from 189 GeV to 209 GeV, corresponding to an integrated luminosity of approximately 600 pb^{-1} . No evidence for excited lepton production was found. In searches for pair-produced excited leptons, lower mass limits were established in the range $94 - 103 \text{ GeV}/c^2$, depending on the channel and model assumptions. In searches for singly-produced excited leptons, upper limits on the parameter f/Λ were established as a function of the mass.

Contributed Paper for LP 2005 (Uppsala) and HEP-EPS 2005 (Lisbon)

Search for excited leptons in e^+e^- collisions at $\sqrt{s} = 189 - 209$ GeV

DELPHI Collaboration

Abstract

A search for excited lepton production in e^+e^- collisions was performed using the data collected by the DELPHI detector at LEP at centre-of-mass energies ranging from 189 GeV to 209 GeV, corresponding to an integrated luminosity of approximately 600 pb^{-1} . No evidence for excited lepton production was found. In searches for pair-produced excited leptons, lower mass limits were established in the range $94 - 103 \text{ GeV}/c^2$, depending on the channel and model assumptions. In searches for singly-produced excited leptons, upper limits on the parameter f/Λ were established as a function of the mass.

(Submitted to Euro. Phys. Jour. C)

J.Abdallah²⁵, P.Abreu²², W.Adam⁵¹, P.Adzic¹¹, T.Albrecht¹⁷, T.Alderweireld², R.Aleman-Fernandez⁸, T.Allmendinger¹⁷, P.P.Allport²³, U.Amaldi²⁹, N.Amapane⁴⁵, S.Amato⁴⁸, E.Anashkin³⁶, A.Andreaazza²⁸, S.Andringa²², N.Anjos²², P.Antilogus²⁵, W-D.Apel¹⁷, Y.Arnaud¹⁴, S.Ask²⁶, B.Asman⁴⁴, J.E.Augustin²⁵, A.Augustinus⁸, P.Baillon⁸, A.Ballestrero⁴⁶, P.Bambade²⁰, R.Barbier²⁷, D.Bardin¹⁶, G.J.Barker¹⁷, A.Baroncelli³⁹, M.Battaglia⁸, M.Baumbach²⁵, K-H.Becks⁵³, M.Begalli⁶, A.Behrmann⁵³, E.Ben-Haim²⁰, N.Benekos³², A.Benvenuti⁵, C.Berat¹⁴, M.Berggren²⁵, L.Berntzon⁴⁴, D.Bertrand², M.Besancon⁴⁰, N.Besson⁴⁰, D.Bloch⁹, M.Blom³¹, M.Bluj⁵², M.Bonesini²⁹, M.Boonekamp⁴⁰, P.S.L.Booth²³, G.Borisov²¹, O.Botner⁴⁹, B.Bouquet²⁰, T.J.V.Bowcock²³, I.Boyko¹⁶, M.Bracko⁴³, R.Brenner⁴⁹, E.Brodet³⁵, P.Bruckman¹⁸, J.M.Brunet⁷, L.Bugge³³, P.Buschmann⁵³, M.Calvi²⁹, T.Camporesi⁸, V.Canale³⁸, F.Carena⁸, N.Castro²², F.Cavallo⁵, M.Chapkin⁴², Ph.Charpentier⁸, P.Checchia³⁶, R.Chierici⁸, P.Chliapnikov⁴², J.Chudoba⁸, S.U.Chung⁸, K.Cieslik¹⁸, P.Collins⁸, R.Contri¹³, G.Cosme²⁰, F.Cossutti⁴⁷, M.J.Costa⁵⁰, D.Crennell³⁷, J.Cuevas³⁴, J.D'Hondt², J.Dalmau⁴⁴, T.da Silva⁴⁸, W.Da Silva²⁵, G.Della Ricca⁴⁷, A.De Angelis⁴⁷, W.De Boer¹⁷, C.De Clercq², B.De Lotto⁴⁷, N.De Maria⁴⁵, A.De Min³⁶, L.de Paula⁴⁸, L.Di Ciaccio³⁸, A.Di Simone³⁹, K.Doroba⁵², J.Drees^{53,8}, M.Dris³², G.Eigen⁴, T.Ekelof⁴⁹, M.Ellert⁴⁹, M.Elsing⁸, M.C.Espirito Santo²², G.Fanourakis¹¹, D.Fassouliotis^{11,3}, M.Feindt¹⁷, J.Fernandez⁴¹, A.Ferrer⁵⁰, F.Ferro¹³, U.Flagmeyer⁵³, H.Foeth⁸, E.Fokitis³², F.Fulda-Quenzer²⁰, J.Fuster⁵⁰, M.Gandelman⁴⁸, C.Garcia⁵⁰, Ph.Gavillet⁸, E.Gaziz³², R.Gokieli^{8,52}, B.Golob⁴³, G.Gomez-Ceballos⁴¹, P.Goncalves²², E.Graziani³⁹, G.Grosdidier²⁰, K.Grzelak⁵², J.Guy³⁷, C.Haag¹⁷, A.Hallgren⁴⁹, K.Hamacher⁵³, K.Hamilton³⁵, S.Haug³³, F.Hauler¹⁷, V.Hedberg²⁶, M.Hennecke¹⁷, H.Herr⁸, J.Hoffman⁵², S-O.Holmgren⁴⁴, P.J.Holt⁸, M.A.Houlden²³, K.Hultqvist⁴⁴, J.N.Jackson²³, G.Jarlskog²⁶, P.Jarry⁴⁰, D.Jeans³⁵, E.K.Johansson⁴⁴, P.D.Johansson⁴⁴, P.Jonsson²⁷, C.Joram⁸, L.Jungermann¹⁷, F.Kapusta²⁵, S.Katsanevas²⁷, E.Katsoufis³², G.Kernel⁴³, B.P.Kersevan^{8,43}, U.Kerzel¹⁷, A.Kiiskinen¹⁵, B.T.King²³, N.J.Kjaer⁸, P.Kluit³¹, P.Kokkinias¹¹, C.Kourkouvelis³, O.Kouznetsov¹⁶, Z.Krumstein¹⁶, M.Kucharczyk¹⁸, J.Lamsa¹, G.Leder⁵¹, F.Ledroit¹⁴, L.Leinonen⁴⁴, R.Leitner³⁰, J.Lemonne², V.Lepeltier²⁰, T.Lesiak¹⁸, W.Liebig⁵³, D.Liko⁵¹, A.Lipniacka⁴⁴, J.H.Lopes⁴⁸, J.M.Lopez³⁴, D.Loukas¹¹, P.Lutz⁴⁰, L.Lyons³⁵, J.MacNaughton⁵¹, A.Malek⁵³, S.Maltezos³², F.Mandl⁵¹, J.Marco⁴¹, R.Marco⁴¹, B.Marechal⁴⁸, M.Margoni³⁶, J-C.Marin⁸, C.Mariotti⁸, A.Markou¹¹, C.Martinez-Rivero⁴¹, J.Masik¹², N.Mastroyiannopoulos¹¹, F.Matorras⁴¹, C.Matteuzzi²⁹, F.Mazzucato³⁶, M.Mazzucato³⁶, R.Mc Nulty²³, C.Meroni²⁸, E.Migliore⁴⁵, W.Mitaroff⁵¹, U.Mjoernmark²⁶, T.Moa⁴⁴, M.Moch¹⁷, K.Moenig^{8,10}, R.Monge¹³, J.Montenegro³¹, D.Moraes⁴⁸, S.Moreno²², P.Morettini¹³, U.Mueller⁵³, K.Muenich⁵³, M.Mulders³¹, L.Mundim⁶, W.Murray³⁷, B.Muryn¹⁹, G.Myatt³⁵, T.Myklebust³³, M.Nassiakou¹¹, F.Navarria⁵, K.Nawrocki⁵², R.Nicolaidou⁴⁰, M.Nikolenko^{16,9}, A.Oblakowska-Mucha¹⁹, V.Obraztsov⁴², A.Olshevski¹⁶, A.Onofre²², R.Orava¹⁵, K.Osterberg¹⁵, A.Ouraou⁴⁰, A.Oyanguren⁵⁰, M.Paganoni²⁹, S.Paiano⁵, J.P.Palacios²³, H.Palka¹⁸, Th.D.Papadopoulou³², L.Pape⁸, C.Parkes²⁴, F.Parodi¹³, U.Parzefall⁸, A.Passeri³⁹, O.Passon⁵³, L.Peralta²², V.Perepelitsa⁵⁰, A.Perrotta⁵, A.Petrolini¹³, J.Piedra⁴¹, L.Pieri³⁹, F.Pierre⁴⁰, M.Pimenta²², E.Piotto⁸, T.Podobnik⁴³, V.Poireau⁸, M.E.Pol⁶, G.Polok¹⁸, V.Pozdniakov¹⁶, N.Pukhaeva^{2,16}, A.Pullia²⁹, J.Rames¹², A.Read³³, P.Rebecchi⁸, J.Rehn¹⁷, D.Reid³¹, R.Reinhardt⁵³, P.Renton³⁵, F.Richard²⁰, J.Ridky¹², M.Rivero⁴¹, D.Rodriguez⁴¹, A.Romero⁴⁵, P.Ronchese³⁶, P.Roudeau²⁰, T.Rovelli⁵, V.Ruhlmann-Kleider⁴⁰, D.Ryabtchikov⁴², A.Sadovsky¹⁶, L.Salmi¹⁵, J.Salt⁵⁰, C.Sander¹⁷, A.Savoy-Navarro²⁵, U.Schwickerath⁸, A.Segar³⁵, R.Sekulin³⁷, M.Siebel⁵³, A.Sisakian¹⁶, G.Smadja²⁷, O.Smirnova²⁶, A.Sokolov⁴², A.Sopczak²¹, R.Sosnowski⁵², T.Spaso⁸, M.Stanitzki¹⁷, A.Stocchi²⁰, J.Strauss⁵¹, B.Stugu⁴, M.Szczekowski⁵², M.Szeptycka⁵², T.Szumlak¹⁹, T.Tabarelli²⁹, A.C.Taffard²³, F.Tegenfeldt⁴⁹, J.Timmermans³¹, L.Tkatchev¹⁶, M.Tobin²³, S.Todorovova¹², B.Tome²², A.Tonazzo²⁹, P.Tortosa⁵⁰, P.Travnicek¹², D.Treille⁸, G.Tristram⁷, M.Trochimczuk⁵², C.Trincon²⁸, M-L.Turluer⁴⁰, I.A.Tyapkin¹⁶, P.Tyapkin¹⁶, S.Tzamarias¹¹, V.Uvarov⁴², G.Valenti⁵, P.Van Dam³¹, J.Van Eldik⁸, A.Van Lysebetten², N.van Remortel², I.Van Vulpen⁸, G.Vegni²⁸, F.Veloso²², W.Venus³⁷, P.Verdier²⁷, V.Verzi³⁸, D.Vilanova⁴⁰, L.Vitale⁴⁷, V.Vrba¹², H.Wahlen⁵³, A.J.Washbrook²³, C.Weiser¹⁷, D.Wicke⁸,

J.Wickens², G.Wilkinson³⁵, M.Winter⁹, M.Witek¹⁸, O.Yushchenko⁴², A.Zalewska¹⁸, P.Zalewski⁵², D.Zavrtanik⁴³, V.Zhuravlov¹⁶, N.I.Zimin¹⁶, A.Zintchenko¹⁶, M.Zupan¹¹

¹Department of Physics and Astronomy, Iowa State University, Ames IA 50011-3160, USA

²Physics Department, Universiteit Antwerpen, Universiteitsplein 1, B-2610 Antwerpen, Belgium and IIHE, ULB-VUB, Pleinlaan 2, B-1050 Brussels, Belgium

and Faculté des Sciences, Univ. de l'Etat Mons, Av. Maistriau 19, B-7000 Mons, Belgium

³Physics Laboratory, University of Athens, Solonos Str. 104, GR-10680 Athens, Greece

⁴Department of Physics, University of Bergen, Allégaten 55, NO-5007 Bergen, Norway

⁵Dipartimento di Fisica, Università di Bologna and INFN, Via Irnerio 46, IT-40126 Bologna, Italy

⁶Centro Brasileiro de Pesquisas Físicas, rua Xavier Sigaud 150, BR-22290 Rio de Janeiro, Brazil and Depto. de Física, Pont. Univ. Católica, C.P. 38071 BR-22453 Rio de Janeiro, Brazil

and Inst. de Física, Univ. Estadual do Rio de Janeiro, rua São Francisco Xavier 524, Rio de Janeiro, Brazil

⁷Collège de France, Lab. de Physique Corpusculaire, IN2P3-CNRS, FR-75231 Paris Cedex 05, France

⁸CERN, CH-1211 Geneva 23, Switzerland

⁹Institut de Recherches Subatomiques, IN2P3 - CNRS/ULP - BP20, FR-67037 Strasbourg Cedex, France

¹⁰Now at DESY-Zeuthen, Platanenallee 6, D-15735 Zeuthen, Germany

¹¹Institute of Nuclear Physics, N.C.S.R. Demokritos, P.O. Box 60228, GR-15310 Athens, Greece

¹²FZU, Inst. of Phys. of the C.A.S. High Energy Physics Division, Na Slovance 2, CZ-180 40, Praha 8, Czech Republic

¹³Dipartimento di Fisica, Università di Genova and INFN, Via Dodecaneso 33, IT-16146 Genova, Italy

¹⁴Institut des Sciences Nucléaires, IN2P3-CNRS, Université de Grenoble 1, FR-38026 Grenoble Cedex, France

¹⁵Helsinki Institute of Physics, P.O. Box 64, FIN-00014 University of Helsinki, Finland

¹⁶Joint Institute for Nuclear Research, Dubna, Head Post Office, P.O. Box 79, RU-101 000 Moscow, Russian Federation

¹⁷Institut für Experimentelle Kernphysik, Universität Karlsruhe, Postfach 6980, DE-76128 Karlsruhe, Germany

¹⁸Institute of Nuclear Physics PAN, Ul. Radzikowskiego 152, PL-31142 Krakow, Poland

¹⁹Faculty of Physics and Nuclear Techniques, University of Mining and Metallurgy, PL-30055 Krakow, Poland

²⁰Université de Paris-Sud, Lab. de l'Accélérateur Linéaire, IN2P3-CNRS, Bât. 200, FR-91405 Orsay Cedex, France

²¹School of Physics and Chemistry, University of Lancaster, Lancaster LA1 4YB, UK

²²LIP, IST, FCUL - Av. Elias Garcia, 14-1^o, PT-1000 Lisboa Codex, Portugal

²³Department of Physics, University of Liverpool, P.O. Box 147, Liverpool L69 3BX, UK

²⁴Dept. of Physics and Astronomy, Kelvin Building, University of Glasgow, Glasgow G12 8QQ, UK.

²⁵LPNHE, IN2P3-CNRS, Univ. Paris VI et VII, Tour 33 (RdC), 4 place Jussieu, FR-75252 Paris Cedex 05, France

²⁶Department of Physics, University of Lund, Sölvegatan 14, SE-223 63 Lund, Sweden

²⁷Université Claude Bernard de Lyon, IPNL, IN2P3-CNRS, FR-69622 Villeurbanne Cedex, France

²⁸Dipartimento di Fisica, Università di Milano and INFN-MILANO, Via Celoria 16, IT-20133 Milan, Italy

²⁹Dipartimento di Fisica, Univ. di Milano-Bicocca and INFN-MILANO, Piazza della Scienza 2, IT-20126 Milan, Italy

³⁰IPNP of MFF, Charles Univ., Areal MFF, V Holesovickach 2, CZ-180 00, Praha 8, Czech Republic

³¹NIKHEF, Postbus 41882, NL-1009 DB Amsterdam, The Netherlands

³²National Technical University, Physics Department, Zografou Campus, GR-15773 Athens, Greece

³³Physics Department, University of Oslo, Blindern, NO-0316 Oslo, Norway

³⁴Dpto. Física, Univ. Oviedo, Avda. Calvo Sotelo s/n, ES-33007 Oviedo, Spain

³⁵Department of Physics, University of Oxford, Keble Road, Oxford OX1 3RH, UK

³⁶Dipartimento di Fisica, Università di Padova and INFN, Via Marzolo 8, IT-35131 Padua, Italy

³⁷Rutherford Appleton Laboratory, Chilton, Didcot OX11 0QX, UK

³⁸Dipartimento di Fisica, Università di Roma II and INFN, Tor Vergata, IT-00173 Rome, Italy

³⁹Dipartimento di Fisica, Università di Roma III and INFN, Via della Vasca Navale 84, IT-00146 Rome, Italy

⁴⁰DAPNIA/Service de Physique des Particules, CEA-Saclay, FR-91191 Gif-sur-Yvette Cedex, France

⁴¹Instituto de Física de Cantabria (CSIC-UC), Avda. los Castros s/n, ES-39006 Santander, Spain

⁴²Inst. for High Energy Physics, Serpukov P.O. Box 35, Protvino, (Moscow Region), Russian Federation

⁴³J. Stefan Institute, Jamova 39, SI-1000 Ljubljana, Slovenia and Laboratory for Astroparticle Physics, Nova Gorica Polytechnic, Kostanjevska 16a, SI-5000 Nova Gorica, Slovenia,

and Department of Physics, University of Ljubljana, SI-1000 Ljubljana, Slovenia

⁴⁴Fysikum, Stockholm University, Box 6730, SE-113 85 Stockholm, Sweden

⁴⁵Dipartimento di Fisica Sperimentale, Università di Torino and INFN, Via P. Giuria 1, IT-10125 Turin, Italy

⁴⁶INFN, Sezione di Torino, and Dipartimento di Fisica Teorica, Università di Torino, Via P. Giuria 1,

IT-10125 Turin, Italy

⁴⁷Dipartimento di Fisica, Università di Trieste and INFN, Via A. Valerio 2, IT-34127 Trieste, Italy

and Istituto di Fisica, Università di Udine, IT-33100 Udine, Italy

⁴⁸Univ. Federal do Rio de Janeiro, C.P. 68528 Cidade Univ., Ilha do Fundão BR-21945-970 Rio de Janeiro, Brazil

⁴⁹Department of Radiation Sciences, University of Uppsala, P.O. Box 535, SE-751 21 Uppsala, Sweden

⁵⁰IFIC, Valencia-CSIC, and D.F.A.M.N., U. de Valencia, Avda. Dr. Moliner 50, ES-46100 Burjassot (Valencia), Spain

⁵¹Institut für Hochenergiephysik, Österr. Akad. d. Wissensch., Nikolsdorfergasse 18, AT-1050 Vienna, Austria

⁵²Inst. Nuclear Studies and University of Warsaw, Ul. Hoza 69, PL-00681 Warsaw, Poland

⁵³Fachbereich Physik, University of Wuppertal, Postfach 100 127, DE-42097 Wuppertal, Germany

1 Introduction

Excited leptons are predicted by models with substructure in the fermionic sector [1,2]. They are assumed to have spin and weak isospin equal to 1/2 and to have both their left-handed and right-handed components in weak isodoublets:

$$L_L^* = \begin{pmatrix} \nu^* \\ \ell^* \end{pmatrix}_L \quad L_R^* = \begin{pmatrix} \nu^* \\ \ell^* \end{pmatrix}_R$$

where $\nu^* = \nu_e^*, \nu_\mu^*, \nu_\tau^*$ and $\ell^* = e^*, \mu^*, \tau^*$ represent the different flavours of neutral and charged excited leptons respectively. Excited leptons ($L^* \equiv \ell^*, \nu^*$) couple to the photon and/or to the W^\pm and Z^0 gauge bosons according to their quantum numbers and thus could be pair-produced at LEP. Single production in association with their Standard Model (SM) partners ($L \equiv \ell, \nu$) is also possible but the production cross-sections depend on the LL^*V couplings, where V is a gauge boson ($V \equiv \gamma, W^\pm, Z^0$) [3]. Excited leptons with masses up to the centre-of-mass energy (\sqrt{s}) can be sought through the single production mode.

This paper presents results of a search for single and pair production of excited leptons of all flavours using data collected by the DELPHI experiment at LEP at centre-of-mass energies between 189 GeV and 209 GeV. Previous results by DELPHI and the other LEP experiments can be found in references [4–6], while results from the HERA experiments can be found in reference [7]. The paper is organised as follows: section 2 reviews the phenomenology of excited lepton production and decay and its consequences for the experimental strategy; in section 3 a detector overview is given and the data and Monte Carlo simulations are presented; event selection criteria applied to the different search channels are described in section 4 and the results obtained are presented in section 5; finally, a summary is presented in section 6.

2 Production and decay of excited leptons

Pair production of charged excited leptons in e^+e^- collisions could proceed via s -channel γ and Z^0 exchanges, while for excited neutrinos only the Z^0 diagram contributes (figure 1). Pair production of excited electrons or excited electron neutrinos would also be possible through t -channel exchange diagrams. In this case two LL^*V vertices are involved and the contribution to the total production cross-section is expected to be negligible compared to the s -channel exchange diagrams.

Single excited lepton production could result from s -channel γ and Z^0 exchange (figure 1). Important additional contributions from t -channel γ and Z^0 exchange arise for excited electron production, while t -channel W^\pm exchange can be important for the excited electron neutrino. In the t -channel production of excited electrons, the SM spectator electron is emitted at small angles to the colliding beams direction and thus is often not detected.

The $SU(2) \times U(1)$ gauge invariant effective Lagrangian describing the magnetic transition between excited leptons and the SM leptons has the form [2]:

$$\mathcal{L}_{LL^*} = \frac{1}{2\Lambda} \bar{L}^* \sigma^{\mu\nu} \left[g f \frac{\vec{\tau}}{2} \cdot \vec{W}_{\mu\nu} + g' f' \frac{Y}{2} B_{\mu\nu} \right] L_L + \text{hermitian conjugate}$$

where $L^* = L_L^* + L_R^*$ and L_L is the weak isodoublet with the left-handed components of the SM leptons; $\sigma^{\mu\nu}$ is the covariant bilinear tensor, $\vec{\tau}$ are the Pauli matrices, Y is

the weak hypercharge, $\vec{W}_{\mu\nu}$ and $B_{\mu\nu}$ represent the gauge field tensors of SU(2) and U(1) respectively, with g and g' being the corresponding SM coupling constants; the parameter Λ sets the compositeness scale, with f and f' being weight factors associated with the two gauge groups. This Lagrangian is associated to the LL^*V vertex, and describes the single production of excited leptons and their decay branching ratios. The strength of the LL^*V coupling is parameterised through f and f' . Form factors and anomalous magnetic moments of the excited leptons were not considered in the reported analyses. To reduce the number of free parameters it is customary to assume a relation between f and f' , or set one of the parameters to zero. In this paper the relations $f = f'$ and $f = -f'$ were considered. With the assumption $|f| = |f'|$, the single excited lepton production cross-section depends only on the ratio f/Λ and on the excited lepton mass.

Excited leptons with masses above 20 GeV/ c^2 are assumed to decay promptly by radiating a γ , W^\pm or Z^0 boson. Their mean lifetime is predicted to be less than 10^{-15} s in all the studied scenarios, thus for detection purposes excited leptons would essentially decay at the production point. The decay branching ratios are function of the f and f' parameters. Figure 2 shows the decay branching ratios as a function of the excited lepton mass (m_{L^*}) for $f = f'$ and $f = -f'$. For charged excited leptons, the electromagnetic radiative decay is forbidden if $f = -f'$ and the decays proceed exclusively through Z^0 and W^\pm bosons. However, as long as $f \neq -f'$ there is a significant contribution to the total decay width from the electromagnetic radiative decay, even if the difference $|f| - |f'|$ is much smaller than $|f|$. If $f = f'$, the electromagnetic radiative decay branching ratio is close to 100% for m_{L^*} smaller than the W^\pm mass (m_W), but decreases for $m_{L^*} > m_W$ reaching a value of 34% for $m_{L^*} = 200$ GeV/ c^2 . For excited neutrinos the electromagnetic decays are forbidden only if $f = f'$.

Many final state topologies would result from the production and decay of excited leptons. The possible final states involve isolated leptons, isolated photons, particle jets from quark fragmentation, missing energy and missing momentum.

Channel	Final State Topologies	
	Single production	Pair production
$\ell^* \rightarrow \ell\gamma$	$\ell\ell\gamma, (\ell)\ell\gamma$	$\ell\ell\gamma\gamma$
$\ell^* \rightarrow \nu W$	$jj\ell, jj(\ell)$	$jj\ell, jjjj$
$\ell^* \rightarrow \ell Z$	$jj\ell\ell, jj\ell(\ell)$	-
$\nu^* \rightarrow \nu\gamma$	γ	$\gamma\gamma$
$\nu^* \rightarrow \ell W$	$jj\ell, jj(\ell)$	$jj\ell\ell, jj\ell\ell(\ell), jjjj\ell\ell$
$\nu^* \rightarrow \nu Z$	jj	-

Table 1: Analysed final-state topologies corresponding to the different production and decay modes of excited leptons. The spectator or final state SM lepton remaining undetected is indicated by (ℓ).

Table 1 shows the topologies considered in the analysis, for the different L^* production and decay channels. Several of those, although not corresponding directly to the physical final state, are expected to become particularly important in presence of low energy or low polar angle¹ leptons. For these topologies the unseen lepton is shown in parentheses.

¹In DELPHI a right-handed Cartesian coordinate system was used, with the z -axis pointing along the electron beam, the x -axis pointing toward the centre of the LEP ring and the origin at the centre of the detector. The polar angle θ is the angle to the electron beam direction and the azimuthal angle ϕ is the angle measured from the x -axis. In this paper the complementary value ($180^\circ - \theta$) is always also assumed.

The final states arising from the W^\pm or Z^0 leptonic decays in the single production mode and the W^+W^- purely leptonic decays or the Z^0Z^0 final states in the pair production searches were not considered due to their small branching ratio and/or small signal sensitivity. In addition the pair-production search criteria aimed at selecting only the topologies arising from the L^*L^* decays to identical gauge bosons (unmixed decays). No specific criteria were defined to select the final state topologies resulting from mixed decays of the gauge bosons.

3 Detector overview and data samples

The data analysed were collected with the DELPHI detector in the years 1998–2000, at centre-of-mass energies ranging from 189 GeV to 209 GeV and correspond to a total integrated luminosity of 598.7 pb^{-1} , with an average centre-of-mass energy of $\langle \sqrt{s} \rangle \simeq 198.5 \text{ GeV}$. A detailed description of the DELPHI detector can be found in reference [8]. In the year 2000 the centre-of-mass energy varied from 201.5 GeV to 208.8 GeV, with an average value of $\langle \sqrt{s} \rangle \simeq 206 \text{ GeV}$. With the purpose of maximizing the discovery potential, these data were subdivided into centre-of-mass energy bins that were analysed independently. During the year 2000 data taking an irrecoverable failure affected one sector of the central tracking detector (TPC), corresponding to 1/12 of its acceptance. The data recorded under these conditions, approximately 60 pb^{-1} , were analysed as an independent energy bin. The luminosity weighted mean centre-of-mass energy and integrated luminosity for each analysed data set are summarised in table 2. The last column corresponds to the data taken after the TPC damage. In the remainder of the text each centre-of-mass energy bin will be referred to by the nearest integer value and the energy bin corresponding to the data taken after the TPC failure as 206*. For the pair production search only the data taken in year 2000 were used in the analysis. In the single production searches the 6.9 pb^{-1} collected at $\sqrt{s} \sim 208 \text{ GeV}$ were analysed together with the 207 GeV data.

Year	1998	1999				2000			
$\langle \sqrt{s} \rangle \text{ (GeV)}$	188.6	191.6	195.5	199.5	201.6	204.9	206.7	208.2	206.5
$\int \mathcal{L} \text{ (pb}^{-1}\text{)}$	151.8	25.1	76.0	82.6	40.1	79.9	77.1	6.9	59.2

Table 2: Luminosity weighted mean centre-of-mass energy and integrated luminosities for the analysed data. The last column corresponds to the data taken after the TPC damage.

Events from Standard Model processes that might contribute to the background were generated at each centre-of-mass energy using several Monte Carlo programs. $e^+e^- \rightarrow f\bar{f}(\gamma)$ events were generated with KK2F [9] (f = quark or muon), KORALZ [10] (f =tau) and BHWIDE [11] for Bhabha events (f =electron). Four-fermion final states were produced with WPHACT [12], while particular phase space regions of the $e^+e^- \rightarrow e^+e^-f\bar{f}$ process, referred to as two-photon interactions, were generated using PYTHIA [13] for hadronic final states, BDKRC [14] for $e^+e^-\mu^+\mu^-$ and $e^+e^-\tau^+\tau^-$ and BDK [15] for $e^+e^-e^+e^-$ final states. $e^+e^- \rightarrow e^+e^-\gamma$ events, with one electron (positron) scattered at very small polar angles while the positron (electron) and photon have large scattering angles, yield a final state with only one electron (or positron) and one photon detected. Such events, which correspond to a particular region of the Bhabha scattering

phase space not covered by the BHWIDE simulated sample, were generated according to [16]. The process $e^+e^- \rightarrow \gamma\gamma(\gamma)$ was simulated using the generator described in [17].

Excited lepton events were simulated to study the distributions of the relevant kinematic variables and to compute the selection efficiencies of the analyses. Single and pair production events of all excited lepton flavours were generated according to the differential cross-sections defined in reference [2]. Simulated events were produced at the relevant centre-of-mass energies and for several excited lepton masses. In the single production scenario the following masses were considered at all centre-of-mass energies: $m_{L^*} = 100, 125, 150, 170, 180 \text{ GeV}/c^2$; additional masses were produced up to the kinematic limit, with values depending on the centre-of-mass energy of the simulated sample (e.g. at $\sqrt{s} = 188.6 \text{ GeV}$ the additional masses $m_{L^*} = 185, 188 \text{ GeV}/c^2$ were also simulated). In the pair-production samples the following masses were considered: $m_{L^*} = 85, 90, 95, 100$ and $103 \text{ GeV}/c^2$; in addition for $\ell^*\ell^* \rightarrow \nu W\nu W$ the m_{L^*} values between 95 and $103 \text{ GeV}/c^2$ were taken in $1 \text{ GeV}/c^2$ steps.

In all simulations the relation $f = f'$ was assumed for the weight factors. However, in the case of the single production of excited electrons, events were generated also with $f = -f'$. This allowed to take into account the strong dependence of the event kinematics on the relative weights of the couplings. In the single-production mode, initial state radiation (ISR) of photons was included at the event generation level, while for the pair-production process it was taken into account in the computation of the total cross-section.

All excited lepton decay modes were included in the single production simulations. For the pair-production the following decays were simulated: $\ell^*\ell^* \rightarrow \ell\ell\gamma\gamma$, $\nu^*\nu^* \rightarrow \nu\nu\gamma\gamma$, $\ell^*\ell^* \rightarrow \nu W\nu W$ and $\nu^*\nu^* \rightarrow \ell W\ell W$. Finally the decays of the SM heavy gauge bosons and tau leptons and the hadronization/fragmentation in hadronic final states were performed using JETSET 7.4 [13].

The generated signal and background events were passed through the detailed simulation of the DELPHI detector and then processed with the same reconstruction and analysis programs as the real data [8]. For the data collected after the TPC failure the reconstruction software for charged particle tracks was adjusted to make best use of the Silicon Tracker and Inner Detector, both placed closer to the beam than the TPC, and the Outer Detector and Barrel Rich, placed outside the TPC. As a result, the impact of the malfunctioning TPC sector on the determination of jet momenta was not large. A dedicated simulation of the detector conditions during this period was also used.

4 Event selection

The production and decay of excited leptons would imply topologies involving isolated leptons, isolated photons, jets and missing energy, as detailed in table 1.

In the first step of the analysis isolated particles were searched by constructing double cones centred in the direction of the charged particle tracks and the neutral energy deposits, defined as energy deposits in the calorimeters not matched to charged particle tracks. The energy detected inside an inner cone with half opening angle of 5° was required to be above 5 GeV, while the energy contained between the inner cone and the outer cone was required to be small, to ensure isolation. Both the opening angle of the outer cone and the maximal accepted total energy contained between the two cones were varied according to the topology of the event and to the energy and identification of the reconstructed particle [18].

Events were pre-selected by requiring the total energy deposited above 20° in polar angle to be greater than $0.2\sqrt{s}$. The events were then classified in different topologies

according to their multiplicity and to the number of isolated leptons and photons. The “low multiplicity” events were required to contain at most five well-reconstructed tracks while “high multiplicity” events contained more than five such tracks. In “low multiplicity” events all particles not identified as isolated photons were clustered into jets using the Durham algorithm [19]. This allowed to treat the tau leptons decays as low multiplicity jets. The jets in the event were obtained by requiring that the jet resolution variable was greater than 0.003 for all jet pairings [5]. If the number of jets thus obtained was smaller than the number of isolated leptons previously found, the jet algorithm was repeated requiring the number of jets to be equal to the number of isolated leptons. Electron, photon and muon identification were based on the standard DELPHI algorithms described in refs. [8,20]. Topology-dependent criteria were then applied, as detailed in the following subsections, and finally the flavour of the final state leptons was used whenever it provided information on the flavour of the excited lepton being searched for.

4.1 Topologies with only photons

Final state topologies consisting of photons only could arise from the production of excited neutrinos decaying to a SM neutrino and a photon. For these topologies the analyses presented in [18,21] were used.

In the search for single production of excited neutrinos, events consisting of only one photon in DELPHI (single photon events) were selected. For the single photon preselection the results from reference [21] were used. The background from SM processes giving single photon events is mainly due to the process $e^+e^- \rightarrow Z^0\gamma \rightarrow \nu\bar{\nu}\gamma$, where the final state photon is emitted predominantly at small polar angles. Candidate events were required to have a photon with polar angle $\theta_\gamma > 45^\circ$ and with energy $E_\gamma > 0.45\sqrt{s}$. In the $\nu\nu^*$ search the data from year 2000 was grouped in two bins, corresponding to $\sqrt{s} < 206$ GeV and $\sqrt{s} > 206$ GeV.

For the $\nu^*\nu^*$ search events with two photons were selected. The analysis used in the selection of two photons and missing energy described in reference [18] was followed, except for the kinematic fit imposing the Z^0 mass on the invisible system and the requirement on the missing mass.

4.2 Topologies with leptons and photons

Topologies with isolated leptons and photons are expected whenever the excited charged leptons decay by photon emission.

For the single production search the topologies $\ell\ell\gamma$ and $\ell\gamma$ were considered as shown in table 1. The $\ell\gamma$ topology becomes dominant for all flavours when the excited lepton mass is close to the centre-of-mass energy. The spectator SM lepton has then too small an energy to be identified as an isolated particle. The $\ell\gamma$ topology is also crucial for the single e^* search when t -channel production dominates, in particular for the $f = f'$ scenario. The SM spectator electron would then be predominantly scattered at small polar angles and would remain undetected.

Different preselection criteria were applied, according to the event classification in each of the topologies and taking into account the relevant background processes and the specific kinematics of the signal events.

Only events with at least one photon with energy $E_\gamma > 0.05\sqrt{s}$ were considered while for the lepton momentum (p_ℓ) it was required $p_\ell > 0.05\sqrt{s}$ in the topologies with only one lepton. In the $\ell\ell\gamma$ topology the sum of the two lepton momenta had to be greater

than $0.1\sqrt{s}$ and the sum of the lepton and photon energies had to be greater than $0.4\sqrt{s}$. In addition, in the e^* and μ^* searches, the momentum of the most energetic lepton had to be greater than $0.05\sqrt{s}$. For events in the $\ell\gamma$ topology it was required that $E_\gamma > 0.1\sqrt{s}$, $p_\ell > 0.1\sqrt{s}$ and $E_\gamma + p_\ell > 0.4\sqrt{s}$.

Figure 3 shows the distribution, after this preselection, of relevant kinematic variables for each of the topologies considered.

The event selection was further tightened as follows. In the case of the $\ell\gamma$ topology the dominant background arise from Bhabha scattering events with one electron lost at low polar angle or identified as a photon. Requiring the presence of an energetic photon in the central region of the detector is the main rejection criterium. For the e^* and τ^* searches in this topology it was thus required that $\theta_\gamma > 42^\circ$.

The main background for the $\ell\ell\gamma$ topology is due to radiative Bhabha scattering events. Initial state radiation events, where the photon is mainly emitted at small polar angle, were reduced by requiring $\theta_\gamma > 42^\circ$ in the e^* and τ^* searches. The background from final state radiation consists of low energy photons emitted at small angle to the direction of the final state leptons. It was thus required $E_\gamma \cdot \sin \alpha > 0.08\sqrt{s}$, where E_γ is the photon energy and α is the angle between the photon direction and the direction of the nearest particle.

The final state topology consisting of one electron and two photons, $e\gamma\gamma$, was additionally considered in the e^* search. In the t -channel dominated e^* production mode the spectator electron could be scattered at angles covered by the low-angle calorimeter of DELPHI, below the geometrical acceptance of the tracking detectors. This electron would then be reconstructed as a photon. In the selection of $\ell\gamma\gamma$ events it was required that one and only one reconstructed photon had a polar angle $\theta_\gamma < 9^\circ$, while the second photon had to be detected above 25° . The sum of the lepton momentum and photon energies had to be greater than $0.8\sqrt{s}$. The main background for this topology is due to radiative Bhabha scattering events, with one low angle scattered electron being identified as a photon. This background is mostly irreducible. Some reduction of the background level was still achievable by requiring that $p_\ell + E_{\gamma_1} > 0.4\sqrt{s}$, where E_{γ_1} is the energy of the low polar-angle photon.

For the pair production search the $\ell\ell\gamma\gamma$ topology was considered. The expected background is rather low and simpler cuts were applied. Both leptons were required to have a momentum above $10 \text{ GeV}/c$. Events were kept as candidates if a lepton-photon pairing could be found for which the difference between the invariant masses of the two lepton-photon pairs was smaller than $15 \text{ GeV}/c^2$ in the e^* and μ^* searches and less than $20 \text{ GeV}/c^2$ in the τ^* search.

The excited lepton mass can be reconstructed by computing the lepton-photon invariant mass. In the $\ell\gamma\gamma$ topology the photon expected from the decay of an excited lepton is the one detected at high polar angle, while in the $\ell\ell\gamma$ topology both possible lepton-photon pairings were considered. The invariant-mass resolution was improved by rescaling the measured energies and momenta. This was done imposing energy-momentum conservation and using just the polar and azimuthal angles, which are well measured in the detector. Resolution of $\pm 1 \text{ mrad}$ in θ and $\pm 1.7 \text{ mrad}$ in ϕ are obtained for high energy photons and of about $\pm 1 \text{ mrad}$ or better in θ and ϕ are obtained for high momentum charged particle tracks, in the central part of the DELPHI detector [8]. In order to take into account the energy lost through initial state radiation, the rescaling was also applied assuming the presence of an additional photon along the beam direction. This procedure accounts also for the case when the spectator electron is lost in the beam pipe. The compatibility of the rescaled and the measured values was quantified through the variable χ^2 ,

defined as:

$$\chi^2 = \frac{1}{n} \sum_{i=1,n} \left(\frac{p_i^{calc} - p_i^{meas}}{\sigma_i} \right)^2$$

where n is the number of particles, p_i^{meas} are the measured momenta or energies and p_i^{calc} are the values calculated from the kinematic constraint; σ_i , the quadratic sum of the errors on p_i^{calc} and p_i^{meas} , is defined in reference [4]. The χ^2 was computed separately for charged particles ($\chi_{charged}^2$) and photons ($\chi_{photons}^2$). The result from the rescaling assuming an additional particle along the beam direction was retained whenever it yielded a smaller total χ^2 . In any case only events with $\min(\chi_{charged}^2, \chi_{photons}^2) < 5$ were retained. The resolution on the lepton-photon invariant mass, after applying the kinematic constraints, was found to be in the range 0.2-0.6 GeV/ c^2 for electrons and muons, and 1.5-2.0 GeV/ c^2 for taus.

Finally, the flavour of the final state leptons was used to select the candidate events. In the e^* search all leptons had to be identified as electrons. The μ^* search criteria required that the most energetic lepton was identified as a muon and no particle was identified as an electron. In the τ^* search no lepton flavour identification was applied. Instead a difference between the measured and rescaled momenta of the final state leptons, characteristic of the presence of neutrinos from tau decays, was required by imposing $\chi_{charged}^2 > 5$ ($\chi_{charged}^2 > 10$ in the $\ell\ell\gamma\gamma$ topology).

4.3 Topologies with jets and leptons

4.3.1 Single production analysis

Final state topologies with jets and isolated leptons were considered in the search for excited leptons decaying to W^\pm or Z^0 , $\ell^* \rightarrow \nu W$, $\ell^* \rightarrow \ell Z^0$, $\nu^* \rightarrow \ell W$ and $\nu^* \rightarrow \nu Z^0$. Due to the presence of neutrinos, some of the topologies are additionally characterized by missing energy. Only the final states arising from the hadronic decays of the W^\pm and Z^0 bosons were studied. Depending on the search channel, up to two isolated leptons could be present. The topologies considered in the single production search were thus jj , $jj\ell$ and $jj\ell\ell$. All particles in the event, excluding the isolated leptons, were clustered into jets using the Durham algorithm. Two-jet events were selected by requiring the jet resolution variable for the transition from three to two jets, y_{23} , to be lower than 0.06 and from two to one jet, y_{12} , to be greater than 0.01. The polar angle of isolated leptons had to be above 25° .

The searches for pair-production of excited leptons already excluded L^* masses smaller than the mass of the Z^0 boson for all excited lepton flavours. The gauge bosons are thus expected to be produced on-shell and the invariant mass of the two jets (M_{jj}) should be compatible with a W^\pm or Z^0 boson. The loose condition $40 < M_{jj} < 120$ GeV/ c^2 was thus applied in all topologies. In addition, since the gauge bosons originating from excited lepton decays are not at rest, the two jets are also expected to be acoplanar. This characteristic is quantified by the jet-jet acoplanarity, A_{cop}^{jj} , defined as $180^\circ - \Phi$, where Φ is the angle between the projections of the jet momenta in the plane perpendicular to the beam.

For events in the jj topology the main background comes from $e^+e^- \rightarrow q\bar{q}(\gamma)$ events, where the photon is emitted at a very small polar angle or is soft, and thus remains undetected. Since the transverse momentum of the photon is always very small (typically < 2 GeV/ c at $\sqrt{s} = 200$ GeV), this process results in two jets with small acoplanarity.

Candidate events were required to have $A_{cop}^{jj} > 25^\circ$ and the polar angle of both jets had to be larger than 20° .

A looser acoplanarity cut, $A_{cop}^{jj} > 10^\circ$, was applied to events in the $jj\ell$ topology. The background is mainly due to W^+W^- production, with one boson decaying to quarks and the other to a charged lepton and a neutrino (W^\pm semileptonic decays). The quantity $\xi = Q_W \cdot \cos\theta_W$, Q_W and θ_W being the boson charge and polar angle respectively, was used to reduce the W^+W^- background. The W^\pm bosons in background events are produced preferentially in the forward direction and ξ is peaked towards -1. In W^\pm semileptonic decays Q_W was given by the lepton charge and θ_W was estimated, neglecting radiation effects, from the jet directions. Events in the $jj\ell$ topology were required to satisfy $\xi > -0.6$, whenever the lepton charge was unambiguously determined.

In the $jj\ell\ell$ topology the angle between the two lepton directions or between any of the leptons and the jet directions had to be greater than 10° . No acoplanarity cut was applied.

Figure 4 shows the distributions for the jet-jet acoplanarity, the variable ξ for events with the lepton charge unambiguously determined and the energy of the most energetic lepton, for the jj , $jj\ell$ and $jj\ell\ell$ topologies, after the preselection cuts.

In order to improve the estimation of the jet momenta and energies a kinematic constrained fit [22] was applied to the selected events. Events in the jj and $jj\ell$ topologies can arise from excited lepton decays mediated by a W^\pm or Z^0 boson and thus the invariant mass of the jet-jet system was constrained to be either m_W or m_Z , depending on the search channel. For events in the $jj\ell\ell$ topology only the m_Z constraint was imposed. In all cases, only the events compatible with the expected decay mode were retained by requiring that the kinematic fit yielded a χ^2 per degree of freedom lower than 5.

The excited lepton mass was estimated in several of the topologies considered. The relevant variables used were the jet-jet-lepton ($\nu\nu^* \rightarrow \nu\ell W^\pm$) and jet-jet-neutrino ($\ell\ell^* \rightarrow \ell\nu W^\pm$) invariant masses, and the recoil mass of isolated leptons ($\ell\ell^* \rightarrow \ell\nu W^\pm$, $\ell\ell^* \rightarrow \ell\ell Z^0$). The resolution on the jet-jet-neutrino invariant mass was found to vary between $1 \text{ GeV}/c^2$ and $5 \text{ GeV}/c^2$. In the $\tau\tau^* \rightarrow \tau\nu W^\pm$ channel, the τ^* mass was reconstructed only for signal masses $m_{\tau^*} > 0.9\sqrt{s}$ and was obtained from the recoil mass of the spectator lepton; the resolution ranged between $3 \text{ GeV}/c^2$ and $6 \text{ GeV}/c^2$. The resolution on the jet-jet-lepton invariant mass was about $2 \text{ GeV}/c^2$ for $m_{\nu^*} = 100 \text{ GeV}/c^2$, increasing to about $10 \text{ GeV}/c^2$ for $m_{\nu^*} = 200 \text{ GeV}/c^2$; no mass reconstruction was attempted in the ν_τ^* channel.

In the last step of the analysis, the various production and decay modes within the same topology were treated differently. In the search for excited leptons of the first or second family, the flavour of the final state leptons had to match the excited lepton flavour. In the case of the $\tau^* \rightarrow \tau Z^0$ search, the lepton energy had to be lower than $0.3\sqrt{s}$ for events in the $jj\ell$ topology, while in $jj\ell\ell$ events at least one lepton with energy lower than $0.2\sqrt{s}$ was required. In $\nu_\tau^* \rightarrow \tau W^\pm$ events, the lepton energy had to be lower than $0.2\sqrt{s}$.

4.3.2 Pair production analysis

$\nu^*\nu^*$ search

In the search for pair production of neutral excited leptons decaying to W^\pm bosons ($\nu^*\nu^* \rightarrow \ell W \ell W$) only the fully hadronic and semileptonic decays of W^+W^- pairs were taken into account. The final state topologies are formed by the W^+W^- decay products

(two jets and one lepton or four jets) and by two additional charged leptons, yielding a rather clear signature.

Multijet events were selected requiring $y_{12} > 0.03$. Events with at least two isolated leptons were kept. If exactly two isolated leptons were found it was further required that $y_{23} > 0.01$.

In the search for ν_e^* and ν_μ^* , the final state had to contain at least two charged leptons of the corresponding flavour. For the ν_τ^* search the missing energy was required to be greater than $0.1\sqrt{s}$.

$\ell^*\ell^*$ search

The final-state topologies considered in the search for pair production of charged excited leptons decaying to W^\pm bosons ($\ell^*\ell^* \rightarrow \nu W\nu W$) were four jets or two jets and one lepton. They result respectively from the fully hadronic or semileptonic decays of the W^+W^- pair.

Contrary to the $\nu^*\nu^*$ search described above, the two additional particles in the final state are now neutrinos, giving missing energy. Signal events have thus a signature very similar to the W^+W^- background events. A discriminant analysis was used in the $\ell^*\ell^* \rightarrow \nu W\nu W$ search, in order to boost the small differences between the signal and background kinematics. After the event preselection a signal likelihood, \mathcal{L}_S , and a background likelihood, \mathcal{L}_B , were constructed as the product of probability density functions (PDFs) of relevant kinematic variables, as described below. The discriminant variable was defined as $\mathcal{L}_S/\mathcal{L}_B$.

The semileptonic and the fully hadronic cases were treated separately. In the semileptonic analysis, events with no isolated photons and at least one isolated lepton were considered. The remaining particles in the event were clustered into jets. Two-jet events were selected by requiring that the Durham resolution variables satisfied the criteria $y_{23} < 0.06$ and $y_{12} > 0.01$. The background from $e^+e^- \rightarrow q\bar{q}(\gamma)$ events was reduced by requiring the polar angle of the direction of the missing momentum to be above 20° . The minimum transverse momentum of the lepton with respect to any of the jets had to be greater than $10 \text{ GeV}/c$; the lepton polar angle was required to be above 20° for muons and above 40° for electrons. The following variables were then used to build the discriminant variable:

- The missing energy of the event;
- The angle between the two jets;
- The energy of the lepton;
- The angle between the lepton and missing momentum directions;
- The $Q_\ell \cdot \cos \theta_\ell$ variable, where Q_ℓ and θ_ℓ are the charge and polar angle of the lepton.

In the fully hadronic analysis it was required that no isolated photons or leptons were present. Four-jet events were selected by requiring $y_{34} > 0.003$ and $y_{23} > 0.03$. The jets were assigned to each of the W^\pm bosons by choosing the pairing that minimized the sum of the squares of the differences between the jet-jet invariant masses and the W^\pm mass. A fit imposing energy-momentum conservation and constraining the invariant mass of the two jet pairs to the W^\pm mass was performed. The following quantities were then used to build the discriminant variable:

- The missing energy of the event;
- The angle between the directions of the two jets of each pair;
- The angle between the two reconstructed W bosons.

The distributions of some of the variables used to build $\mathcal{L}_S/\mathcal{L}_B$ are shown in figure 5. A good agreement with the SM predictions is observed. In figure 6 are shown the distributions of $\mathcal{L}_S/\mathcal{L}_B$ for the semileptonic and the hadronic final states.

5 Results

No evidence for the production of excited leptons was observed in any of the final states that were searched for. The number of candidate events found in the single and pair production searches at the various centre-of-mass energies, together with the expected background from SM processes, are summarized in tables 3 and 4, for the different excited lepton flavours and decay modes. These numbers were obtained by adding the results from the different exclusive final state topologies considered in each decay (as listed in table 1). The relevance of each topology would depend on the decay branching ratios, which are a function of the excited lepton mass and of the coupling parameters. In many cases there are candidate events common to the different excited lepton searches (e.g. the events selected in the jj topology are candidates in all $\ell^* \rightarrow \nu W$ searches, independent of the ℓ^* flavour), but in the search for a given flavour there are no common candidates selected in final states originating from different decay modes.

The signal selection efficiencies for all the studied channels are given in table 5, for specific values of m_{L^*} and at $\sqrt{s} = 206$ GeV. The dependence of the efficiency on the mass is weak, as we benefited from the combination of results from several final state topologies which are sensitive to different mass regions.

Figures 7 and 8 show the invariant mass distributions for the candidates selected in the various single production searches, obtained by adding the data from all the analysed centre-of-mass energies and topologies considered.

5.1 Systematic uncertainties

Systematic uncertainties affect both the background and the signal efficiency estimations.

At the event generation level, errors on the computed cross-sections translate into uncertainties on the expected number of background events. The overall error on the number of background events resulting from the systematic errors on the cross-section of processes contributing significantly to the background is typically less than 2% [23].

The simulated distributions of the kinematic variables used in the event selection may not match the distributions for the data, due either to an imperfect description of the detector or of the background processes at the event generation level. Possible effects on the selected number of simulated events were estimated by studying the change in the ratio between the number of selected events in the data and simulated background, when varying each selection cut around the chosen value, keeping the other cuts fixed: the photon polar angle was varied by $\pm 5^\circ$; the cut in the lepton energy was changed by ± 5 GeV; the jet-jet acoplanarity cut was varied by $\pm 5^\circ$; the limits in the jet-jet invariant mass window were changed by ± 10 GeV. In each topology the contributions from the different selection cuts were added in quadrature resulting in values ranging from 5% to 8%, depending on the topology considered. These were taken as an estimate of the contribution from the analysis cuts to the systematic error on the background expectation. For each final state topology the systematic uncertainties on the signal selection efficiencies due to the selection cuts were assumed to be equal to and fully correlated with the background error.

The statistical errors on the background and signal efficiencies were taken as uncorrelated systematic uncertainties.

An additional source of systematic error on the signal efficiency is due to the description of initial state radiation (ISR) effects at the event generator level. Single production events were generated with collinear ISR only. As long as ISR photons were emitted below the DELPHI acceptance, this would result only in a small change in the event kinematics, with low impact on the signal selection efficiency. However, if the ISR photon was detected, the event topology would be different from the topologies considered in the analysis, resulting in a smaller efficiency for the signal. This effect was estimated using $e^+e^- \rightarrow e^+e^-$ and $e^+e^- \rightarrow \mu^+\mu^-$ simulated events at various centre-of-mass energies. An average correction factor of 0.9 was obtained and was used to rescale the selection efficiencies. The spread on the corrections obtained at the different centre-of-mass energies, of the order of 2%, was taken as an independent contribution to the systematic error of the signal efficiencies.

The systematic uncertainties discussed in this section were included in the computation of the exclusion limits.

5.2 Limits

Limits at 95% confidence level (CL) were computed using the likelihood ratio method described in reference [24]. This method is well suited both for the combination of different search channels and for the inclusion of mass information. Searches in each topology at each centre-of-mass energy were treated as independent channels. Whenever the mass of the particle being searched for could be reconstructed, the PDF for a given signal mass hypothesis was assumed to be Gaussian with mean value equal to the tested signal mass and standard deviation equal to the signal mass resolution. For channels where the excited lepton mass was not reconstructed, all selected events were considered as candidates for all signal mass hypotheses. In the $\ell^*\ell^* \rightarrow \nu W \nu W$ channel, for which a discriminant analysis was performed, the PDFs of the likelihood ratio obtained at each signal mass hypothesis were used.

From the single-production search results, upper limits on the production cross-section multiplied by the decay branching ratio ($\sigma \times \text{BR}$), as a function of the mass, were derived for each excited lepton type and decay mode. These limits are shown in figure 9. As already discussed, the kinematics of single e^* production is sensitive to the contribution from t -channel γ exchange, with impact on the selection efficiencies. Since the $\ell\ell^*\gamma$ coupling becomes significant even for a slight departure from the $f = -f'$ scenario, the e^* limits were computed using the selection efficiencies obtained with $f = f'$. For the other flavours the selection efficiencies do not depend on the f and f' assignments. The limits on $\sigma \times \text{BR}$ can thus be interpreted in broader compositeness scenarios.

The cross-section for single excited lepton production is a function not only of m_{L^*} but also of the coupling parameter f/Λ . The pair production cross-section is a function of m_{L^*} only. Upper limits on f/Λ as a function of m_{L^*} and lower limits on m_{L^*} were derived from the single- and pair-production searches respectively, by combining the results in the various decay modes. The dependence of the decay BR's and production cross-sections on m_{L^*} as given in reference [2] were assumed. The production cross-sections were computed taking into account initial state radiation effects.

Figures 10 and 11 show the limits on f/Λ as a function of m_{L^*} for $f = f'$ and $f = -f'$, respectively. The lower limits on the excited lepton masses are given in table 6 for the two scenarios.

Compositeness can also be probed at LEP through the process $e^+e^- \rightarrow \gamma\gamma(\gamma)$. The additional contribution of the t -channel exchange of a virtual excited electron to the $e^+e^- \rightarrow \gamma\gamma(\gamma)$ cross-section would lead to a change in the angular distribution of the final state photons with respect to the SM prediction. This effect depends on the excited electron mass m_{e^*} and on the $ee^*\gamma$ coupling. The results presented in reference [25] were used to complement the direct searches for the excited electron in the mass region above the kinematic limit for ee^* production. Figure 12 shows the upper limit on f/Λ for the single production of excited electrons with $f = f'$, obtained by taking the best limit of the direct search (figure 10(a)) and the indirect search results, thus extending the excluded region beyond the kinematic limit.

6 Summary

The data collected by DELPHI at $\sqrt{s} = 189-209$ GeV, corresponding to an integrated luminosity of 598.7 pb^{-1} , were analysed to search for excited leptons decaying promptly through γ , Z^0 or W^\pm emission. No evidence for excited lepton production was observed.

The search for L^* pair production resulted in mass limits in the range $94 - 103 \text{ GeV}/c^2$ depending on the excited lepton type and model assumptions, as quoted in table 6. These are close to the kinematic limit for all charged (neutral) excited leptons in the $f = f'$ ($f = -f'$) scenario. From the single production search, limits on f/Λ were set as shown in Figures 10, 11 and 12. Model independent upper bounds on $\sigma \times \text{BR}$ were also derived for each lepton type and decay channel, thus allowing for new interpretations in broader compositeness scenarios. These results confirm and extend the limits set previously at LEP and HERA [5-7].

Acknowledgements

We are greatly indebted to our technical collaborators, to the members of the CERN-SL Division for the excellent performance of the LEP collider, and to the funding agencies for their support in building and operating the DELPHI detector.

We acknowledge in particular the support of

Austrian Federal Ministry of Education, Science and Culture, GZ 616.364/2-III/2a/98,
FNRS-FWO, Flanders Institute to encourage scientific and technological research in the industry (IWT), Belgium,

FINEP, CNPq, CAPES, FUJB and FAPERJ, Brazil,

Czech Ministry of Industry and Trade, GA CR 202/99/1362,

Commission of the European Communities (DG XII),

Direction des Sciences de la Matière, CEA, France,

Bundesministerium für Bildung, Wissenschaft, Forschung und Technologie, Germany,

General Secretariat for Research and Technology, Greece,

National Science Foundation (NWO) and Foundation for Research on Matter (FOM),
The Netherlands,

Norwegian Research Council,

State Committee for Scientific Research, Poland, SPUB-M/CERN/PO3/DZ296/2000,
SPUB-M/CERN/PO3/DZ297/2000, 2P03B 104 19 and 2P03B 69 23(2002-2004),

FCT - Fundação para a Ciência e Tecnologia, Portugal,

Vedecka grantova agentura MS SR, Slovakia, Nr. 95/5195/134,

Ministry of Science and Technology of the Republic of Slovenia,

CICYT, Spain, AEN99-0950 and AEN99-0761,
 The Swedish Research Council,
 Particle Physics and Astronomy Research Council, UK,
 Department of Energy, USA, DE-FG02-01ER41155,
 EEC RTN contract HPRN-CT-00292-2002.

References

- [1] K. Hagiwara, D. Zeppenfeld and S. Komamiya, *Zeit. Phys.* **C29** (1985) 115.
- [2] F. Boudjema, A. Djouadi and J.L. Kneur, *Zeit. Phys.* **C57** (1993) 425.
- [3] A. Djouadi, *Zeit. Phys.* **C63** (1994) 317.
- [4] DELPHI Coll., P. Abreu *et al*, *Phys. Lett.* **B380** (1996) 480.
- [5] DELPHI Coll., P. Abreu *et al*, *Eur. Phys. J.* **C8** (1999) 41.
- [6] ALEPH Coll., R. Barate *et al* *Eur. Phys. J.* **C4** (1998) 571;
 ALEPH Coll., D. Buskulic *et al*, *Phys. Lett.* **B385** (1996) 445;
 L3 Coll., P. Achard *et al*, *Phys. Lett.* **B568** (2003) 23;
 L3 Coll., M. Acciarri *et al*, *Phys. Lett.* **B502** (2001) 37;
 OPAL Coll., G. Abbiendi *et al*, *Phys. Lett.* **B544** (2002) 57;
 OPAL Coll., G. Abbiendi *et al*, *Eur. Phys. J.* **C14** (2000) 73;
- [7] H1 Coll., C. Adloff *et al*, *Phys. Lett.* **B548** (2002) 35;
 H1 Coll., C. Adloff *et al*, *Phys. Lett.* **B525** (2002) 9;
 H1 Coll., C. Adloff *et al*, *Eur. Phys. J.* **C17** (2000) 567;
 ZEUS Coll., S. Chekanov *et al*, *Phys. Lett.* **B549** (2002) 32;
 ZEUS Coll., J. Breitweg *et al*, *Zeit. Phys.* **C76** (1997) 631.
- [8] DELPHI Coll., P. Aarnio *et al*, *Nucl. Instr. Methods* **A303** (1991) 233;
 DELPHI Coll., P. Abreu *et al*, *Nucl. Instr. Methods* **A378** (1996) 57.
- [9] S. Jadach, B.F.L. Ward and Z. Wąs, *Comp. Phys. Comm.* **130** (2000) 260.
- [10] S. Jadach, B.F.L. Ward and Z. Wąs, *Comp. Phys. Comm.* **66** (1991) 276.
- [11] S. Jadach, W. Placzek and B.F.L. Ward, *Phys. Lett.* **B390** (1997) 298.
- [12] E. Accomando and A. Ballestrero, *Comp. Phys. Comm.* **99** (1997) 270;
 E. Accomando, A. Ballestrero and E. Maina, *Comp. Phys. Comm.* **150** (2003) 166.
- [13] T. Sjöstrand *et al*, *Comp. Phys. Comm.* **135** (2001) 238;
 T. Sjöstrand, *Comp. Phys. Comm.* **82** (1994) 74;
 T. Sjöstrand, Pythia 5.7 and Jetset 7.4, Preprint CERN-TH/7112-93 (1993).
- [14] F.A. Berends, P.H. Daverveldt and R. Kleiss, *Comp. Phys. Comm.* **40** (1986) 271.
- [15] F.A. Berends, P.H. Daverveldt and R. Kleiss, *Comp. Phys. Comm.* **40** (1986) 285.
- [16] D. Karlen, *Nucl. Phys.* **B289** (1987) 23.
- [17] F. Berends and R. Kleiss, *Nucl. Phys.* **B186** (1981) 22.
- [18] DELPHI Coll., J. Abdallah *et al*, *Eur. Phys. J.* **C35** (2004) 313.
- [19] S. Catani *et al*, *Phys. Lett.* **B269** (1991) 432.
- [20] F. Cossutti *et al*, “REMCLU: a package for the Reconstruction of Electromagnetic CLUsters at LEP200”, DELPHI Note 2000-164 PROG 242.
- [21] DELPHI Coll., J. Abdallah *et al*, *Eur. Phys. J.* **C38** (2005) 395.
- [22] DELPHI Coll., P. Abreu *et al*, *Eur. Phys. J.* **C2** (1998) 581.
- [23] CERN Report 96-01, vol.2 (1996), “Workshop on Physics at LEP2”, edited by G. Altarelli, T. Sjöstrand and F. Zwirner;
 CERN Report 2000-009 (2000), “LEP2 Monte Carlo Workshop: Report of the Working Groups on Precision Calculations for LEP2 Physics”, edited by S. Jadach, G. Pas-

sarino and R. Pittau.

- [24] A.L. Read, CERN Report 2000-005 (2000) 81, “Workshop on Confidence Limits”, edited by F. James, L. Lyons and Y. Perrin.
- [25] DELPHI Coll., J. Abdallah *et al*, Eur. Phys. J. **C37** (2004) 405.

\sqrt{s} (GeV)	Channel	Excited lepton flavour					
		e		μ		τ	
189	$\ell^* \rightarrow \ell\gamma$	366	(408.2±6.7)	39	(44.0±1.5)	62	(54.3±2.7)
	$\ell^* \rightarrow \nu W^\pm$	202	(217.6±4.8)	195	(195.5±4.3)	432	(447.8±7.1)
	$\ell^* \rightarrow \ell Z^0$	51	(42.0±3.4)	8	(10.00±0.66)	55	(40.9±2.7)
	$\nu^* \rightarrow \nu\gamma$	3 (0.70±0.17)					
	$\nu^* \rightarrow \ell W^\pm$	175	(180.1±4.9)	133	(131.3±3.2)	203	(196.5±4.9)
	$\nu^* \rightarrow \nu Z^0$	75 (81.1±3.1)					
192	$\ell^* \rightarrow \ell\gamma$	61	(66.4±2.0)	8	(7.29±0.27)	10	(8.05±0.76)
	$\ell^* \rightarrow \nu W^\pm$	28	(38.04±0.79)	25	(33.71±0.69)	56	(75.2±1.1)
	$\ell^* \rightarrow \ell Z^0$	5	(5.24±0.44)	1	(2.01±0.16)	3	(6.56±0.43)
	$\nu^* \rightarrow \nu\gamma$	0 (0.10±0.03)					
	$\nu^* \rightarrow \ell W^\pm$	24	(28.53±0.75)	18	(22.01±0.53)	26	(31.33±0.79)
	$\nu^* \rightarrow \nu Z^0$	9 (14.87±0.49)					
196	$\ell^* \rightarrow \ell\gamma$	201	(188.9±3.3)	18	(20.27±0.73)	24	(23.4±1.3)
	$\ell^* \rightarrow \nu W^\pm$	108	(117.3±2.4)	103	(101.6±2.1)	232	(230.0±3.5)
	$\ell^* \rightarrow \ell Z^0$	26	(20.4±1.5)	3	(5.81±0.36)	23	(21.0±1.2)
	$\nu^* \rightarrow \nu\gamma$	2 (0.70±0.08)					
	$\nu^* \rightarrow \ell W^\pm$	90	(91.2±2.3)	72	(64.6±1.6)	106	(96.7±2.4)
	$\nu^* \rightarrow \nu Z^0$	38 (45.6±1.5)					
200	$\ell^* \rightarrow \ell\gamma$	190	(198.8±3.5)	25	(20.74±0.74)	26	(27.3±1.3)
	$\ell^* \rightarrow \nu W^\pm$	128	(131.1±2.6)	102	(114.6±2.4)	239	(248.0±3.7)
	$\ell^* \rightarrow \ell Z^0$	29	(19.3±1.4)	9	(7.05±0.48)	28	(22.4±1.3)
	$\nu^* \rightarrow \nu\gamma$	6 (1.7±0.1)					
	$\nu^* \rightarrow \ell W^\pm$	116	(96.7±2.4)	70	(70.5±1.7)	108	(102.5±2.5)
	$\nu^* \rightarrow \nu Z^0$	42 (52.2±1.7)					
202	$\ell^* \rightarrow \ell\gamma$	87	(94.9±2.1)	8	(9.44±0.38)	16	(12.05±0.73)
	$\ell^* \rightarrow \nu W^\pm$	79	(61.9±1.2)	54	(54.1±1.1)	138	(119.6±1.8)
	$\ell^* \rightarrow \ell Z^0$	5	(10.53±0.77)	4	(3.45±0.25)	9	(11.42±0.68)
	$\nu^* \rightarrow \nu\gamma$	1 (1.2±0.1)					
	$\nu^* \rightarrow \ell W^\pm$	54	(46.8±1.2)	28	(33.57±0.84)	55	(51.4±1.3)
	$\nu^* \rightarrow \nu Z^0$	31 (24.91±0.80)					
205	$\ell^* \rightarrow \ell\gamma$	179	(182.7±3.8)	20	(18.28±0.34)	27	(24.3±1.2)
	$\ell^* \rightarrow \nu W^\pm$	119	(123.8±2.4)	94	(102.4±2.1)	225	(231.5±3.4)
	$\ell^* \rightarrow \ell Z^0$	22	(18.0±1.3)	7	(6.82±0.47)	24	(21.5±1.3)
	$\nu^* \rightarrow \nu\gamma$	5 (1.3±0.2)					
	$\nu^* \rightarrow \ell W^\pm$	98	(90.9±2.3)	60	(61.8±1.6)	88	(100.1±2.4)
	$\nu^* \rightarrow \nu Z^0$	46 (50.5±1.6)					
206*	$\ell^* \rightarrow \ell\gamma$	120	(129.8±2.7)	11	(13.15±0.25)	16	(19.2±1.0)
	$\ell^* \rightarrow \nu W^\pm$	79	(93.9±1.8)	70	(79.8±1.7)	138	(173.1±2.5)
	$\ell^* \rightarrow \ell Z^0$	15	(14.3±1.0)	3	(4.51±0.35)	16	(14.75±0.88)
	$\nu^* \rightarrow \ell W^\pm$	58	(67.4±1.7)	41	(46.4±1.2)	53	(72.3±1.7)
	$\nu^* \rightarrow \nu Z^0$	37 (38.9±1.2)					
> 206	$\nu^* \rightarrow \nu\gamma$	1 (2.6±0.2)					
207 + 208	$\ell^* \rightarrow \ell\gamma$	172	(180.9±3.3)	15	(18.28±0.34)	21	(25.1±1.2)
	$\ell^* \rightarrow \nu W^\pm$	110	(130.6±2.5)	94	(110.7±2.3)	205	(239.3±3.5)
	$\ell^* \rightarrow \ell Z^0$	30	(22.8±1.6)	6	(6.9±0.5)	21	(23.4±1.3)
	$\nu^* \rightarrow \ell W^\pm$	86	(96.4±2.4)	52	(64.9±1.7)	87	(99.9±2.4)
	$\nu^* \rightarrow \nu Z^0$	53 (55.3±1.7)					

Table 3: Number of candidates for the different excited lepton decay channels in the single production search. The numbers in parentheses correspond to the SM background expectations with the statistical errors.

\sqrt{s} (GeV)	Channel	Excited lepton flavour		
		e	μ	τ
205	$\ell^* \rightarrow \ell\gamma$	0 (1.25±0.33)	0 (0.38±0.05)	1 (2.57±0.41)
	$\nu^* \rightarrow \nu\gamma$	4 (3.26±0.33)		
	$\ell^* \rightarrow \nu W$ (hadr.)	403 (419.9±5.1)		
	$\ell^* \rightarrow \nu W$ (semilep.)	261 (231.1±3.1)		
	$\nu^* \rightarrow \ell W$	1 (3.21±0.33)	1 (0.99±0.16)	18 (17.43±0.87)
206*	$\ell^* \rightarrow \ell\gamma$	1 (0.52±0.20)	0 (0.29±0.04)	3 (1.48±0.27)
	$\nu^* \rightarrow \nu\gamma$	6 (2.21±0.26)		
	$\ell^* \rightarrow \nu W$ (hadr.)	280 (311.0±3.8)		
	$\ell^* \rightarrow \nu W$ (semilep.)	154 (176.6±2.4)		
	$\nu^* \rightarrow \ell W$	6 (2.56±0.32)	0 (0.93±0.14)	15 (12.04±0.61)
207	$\ell^* \rightarrow \ell\gamma$	1 (1.49±0.34)	2 (0.41±0.05)	3 (2.59±0.39)
	$\nu^* \rightarrow \nu\gamma$	3 (3.50±0.36)		
	$\ell^* \rightarrow \nu W$ (hadr.)	408 (416.9±5.0)		
	$\ell^* \rightarrow \nu W$ (semilep.)	228 (239.0±3.2)		
	$\nu^* \rightarrow \ell W$	3 (3.10±0.32)	1 (1.74±0.22)	20 (17.22±0.89)
208	$\ell^* \rightarrow \ell\gamma$	0 (0.16±0.06)	0 (0.04±0.01)	0 (0.25±0.07)
	$\nu^* \rightarrow \nu\gamma$	-		
	$\ell^* \rightarrow \nu W$ (hadr.)	34 (34.95±0.85)		
	$\ell^* \rightarrow \nu W$ (semilep.)	10 (19.94±0.54)		
	$\nu^* \rightarrow \ell W$	0 (0.36±0.08)	0 (0.10±0.02)	2 (1.68±0.17)

Table 4: Number of excited lepton candidates for the different decay channels and the different centre-of-mass energies in the pair production search. The numbers in parentheses correspond to the SM background expectations with the statistical errors.

channel	Excited lepton flavour		
	e	μ	τ
Single production			
$\ell^* \rightarrow \ell\gamma$	40.3±2.0	61.2±2.5	22.5±1.5
$\ell^* \rightarrow \nu W$	33.1±1.8	32.9±1.8	43.3±2.1
$\ell^* \rightarrow \ell Z$	19.7±1.4	41.7±2.0	19.6±1.4
$\nu^* \rightarrow \nu\gamma$	32.5±1.8		
$\nu^* \rightarrow \ell W$	34.1±1.8	34.2±1.8	18.0±1.3
$\nu^* \rightarrow \nu Z$	40.7±2.0		
Pair production			
$\ell^* \rightarrow \ell\gamma$	38.2 ±1.4	50.8 ±1.6	17.5 ±0.9
$\ell^* \rightarrow \nu W$ (hadr.)	22.1±0.7		
$\ell^* \rightarrow \nu W$ (semilep.)	16.3±0.6		
$\nu^* \rightarrow \nu\gamma$	52.9±2.3		
$\nu^* \rightarrow \ell W$	27.9±1.7	42.3±2.1	13.1±1.1

Table 5: Selection efficiencies (in %) for the different excited lepton flavours and decay channels, in the single (top) and pair (bottom) production modes. Efficiencies are quoted for excited lepton masses of $m_{L^*}=200$ GeV/ c^2 in the single production and $m_{L^*}=100$ GeV/ c^2 in the pair production, at $\sqrt{s}=206$ GeV.

	e^*	μ^*	τ^*		ν_e^*	ν_μ^*	ν_τ^*
$f = f'$	103.1	103.2	102.7	$f = f'$	101.9	103.2	94.2
$f = -f'$	101.0	101.0	101.0	$f = -f'$	101.9	102.2	101.9

Table 6: Lower limits (in GeV/c^2) at 95 % CL on the excited lepton masses obtained from the pair production searches.

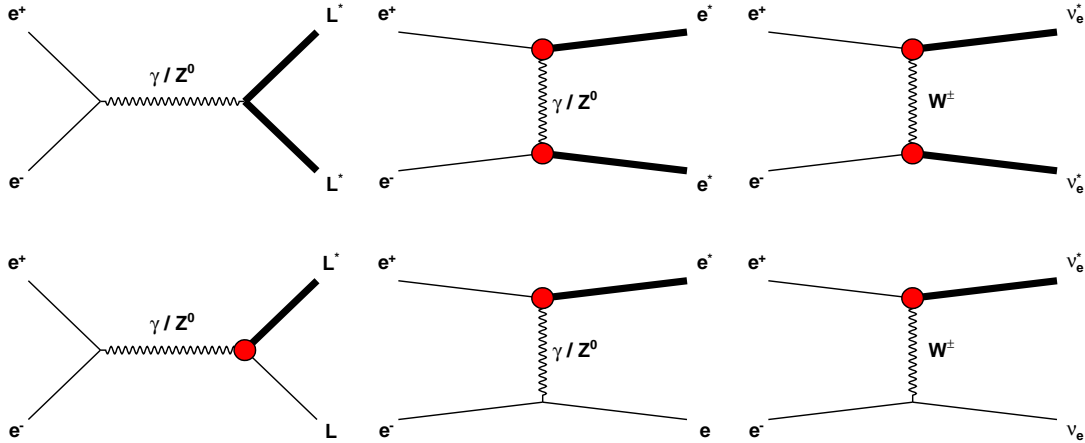


Figure 1: Feynman diagrams for the double (top) and single (bottom) excited lepton production. Each L^* is shown as a thicker line. The vertex shown as a closed circle represents a LL^*V coupling ($V \equiv \gamma, W^\pm, Z^0$) inversely proportional to the compositeness scale parameter Λ .

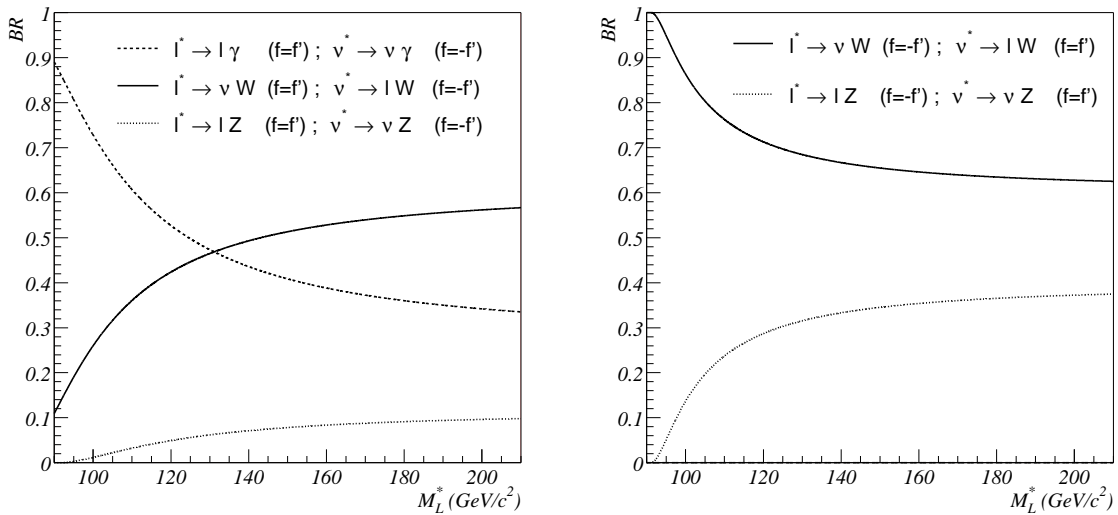


Figure 2: Branching ratios of the excited lepton decays as a function of the mass. In the left plot are shown the branching ratios for charged and neutral excited leptons when $f = f'$ and $f = -f'$, respectively. The right plot refers to the symmetric f and f' couplings assignment.

DELPHI

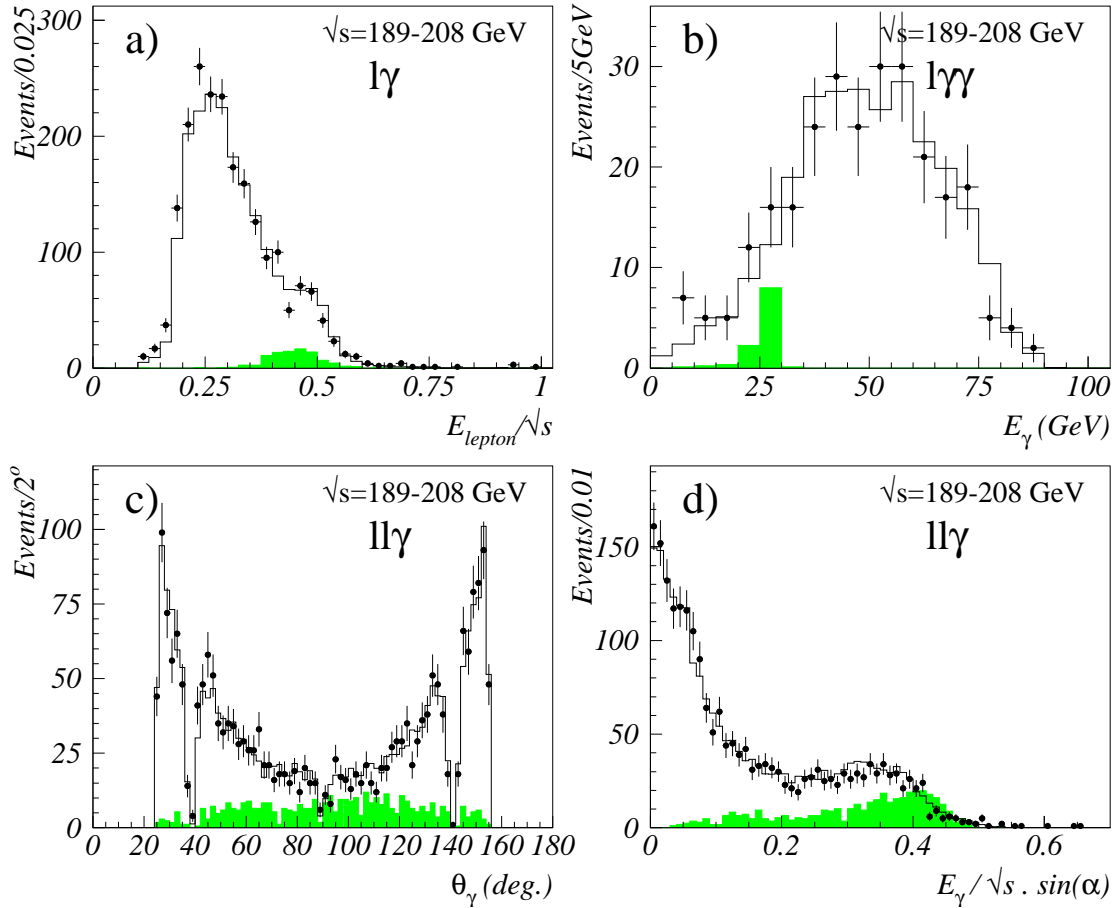


Figure 3: Topologies with leptons and photons after the preselection cuts: **(a)** lepton energy in the $l\gamma$ topology; **(b)** energy of the least energetic photon in the $l\gamma\gamma$ topology; **(c)** photon polar angle and **(d)** $E_\gamma/\sqrt{s} \cdot \sin(\alpha)$, where α is the minimum angle between the photon direction and the two lepton directions, in the $ll\gamma$ topology. The dots show the data and the white histograms show the SM simulation. The shaded histograms show the expected distributions for a $m_{L^*} = 175 \text{ GeV}/c^2$ excited lepton at $\sqrt{s} = 206 \text{ GeV}$, using an arbitrary normalization.

DELPHI

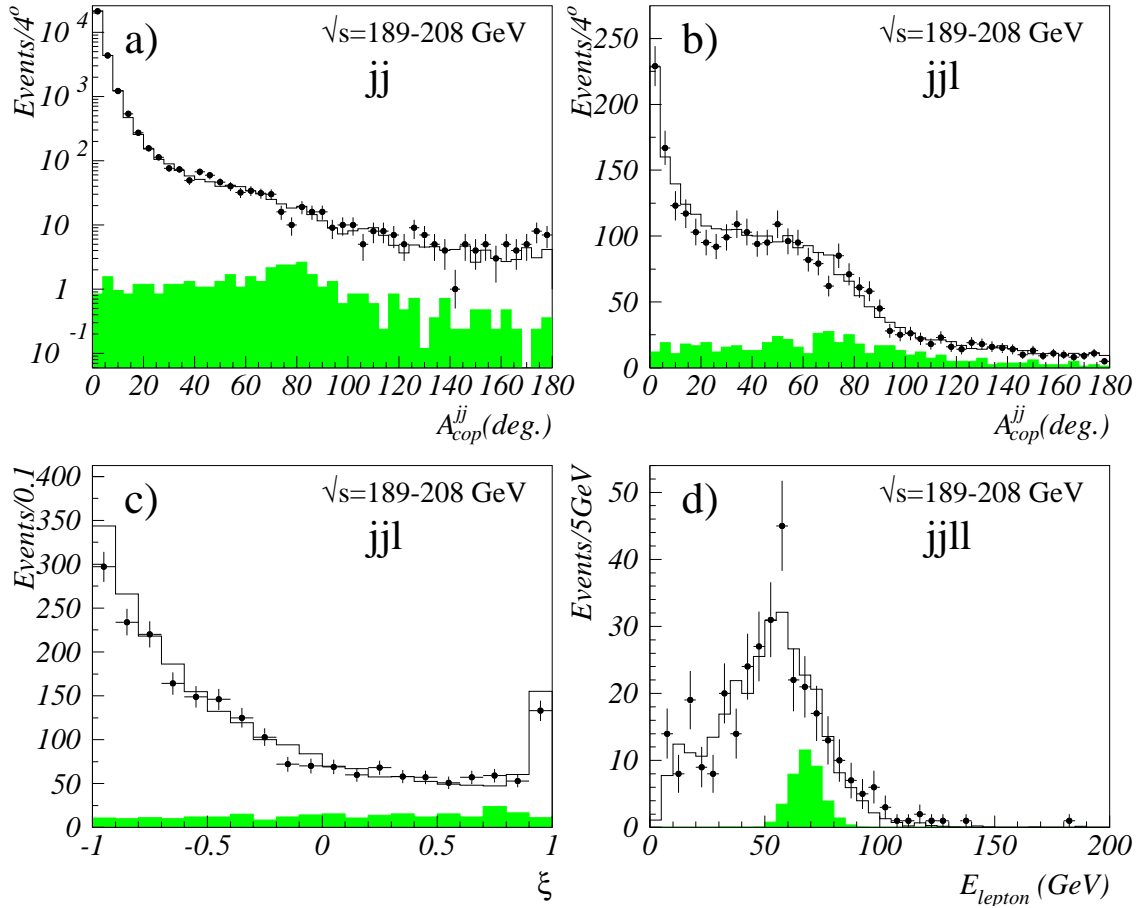


Figure 4: Topologies with jets and leptons after the preselection cuts: **(a)** jet-jet acoplanarity in the jj topology; **(b)** jet-jet acoplanarity in the jjl topology; **(c)** variable $\xi = Q_W \cdot \cos\theta_W$ in the jjl topology, for events with the lepton charge unambiguously determined; **(d)** energy of the most energetic lepton in $jjll$ events. The dots show the data and the white histograms show the SM simulation. The shaded histograms show the expected distributions for a $m_{L^*} = 175$ GeV/ c^2 excited lepton at $\sqrt{s} = 206$ GeV, using an arbitrary normalization.

DELPHI

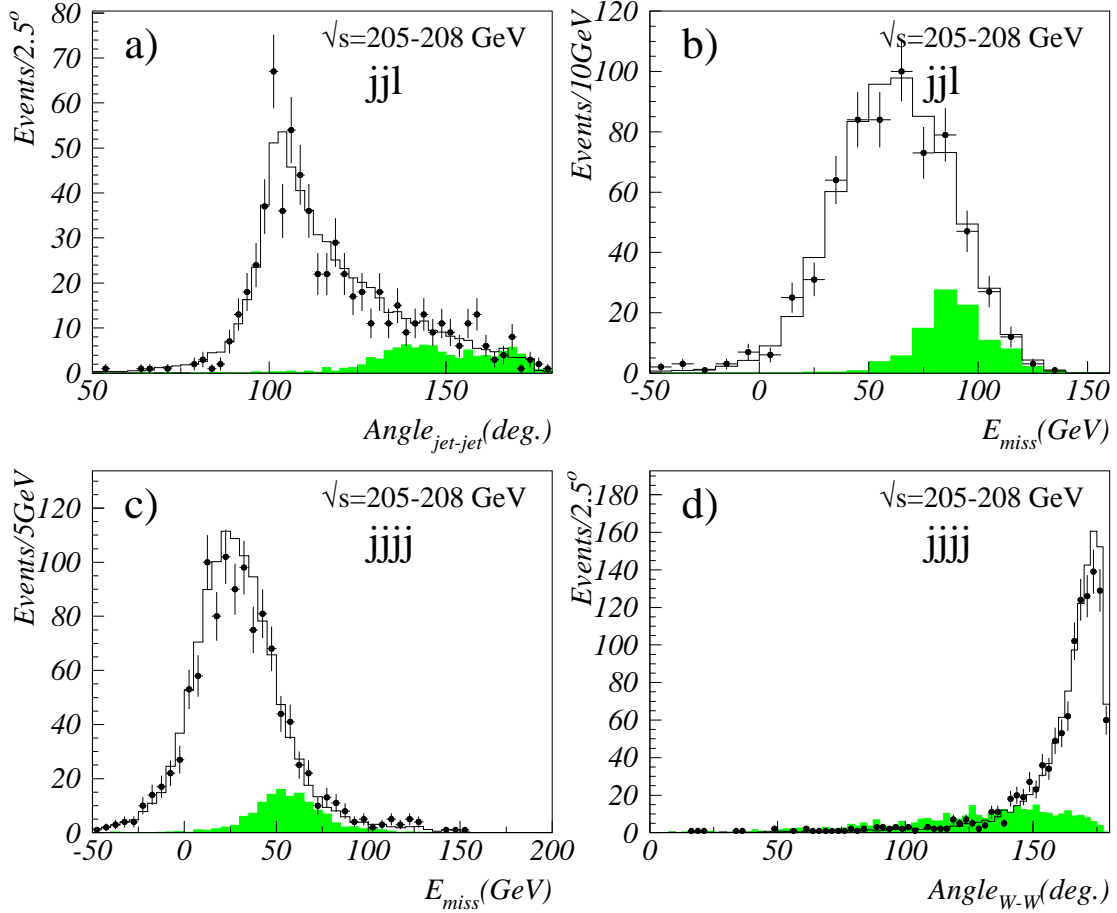


Figure 5: $\ell^*\ell^*$ search at the preselection level: (a) angle between the two jets and (b) missing energy in the semileptonic channel; (c) missing energy and (d) angle between the two reconstructed W s in the fully hadronic channel. The dots show the data and the white histograms show the expected SM background. The shaded histograms show the expected signal distributions at $\sqrt{s} = 206$ GeV with $m_{L^*} = 100$ GeV/ c^2 , using an arbitrary normalization.

DELPHI

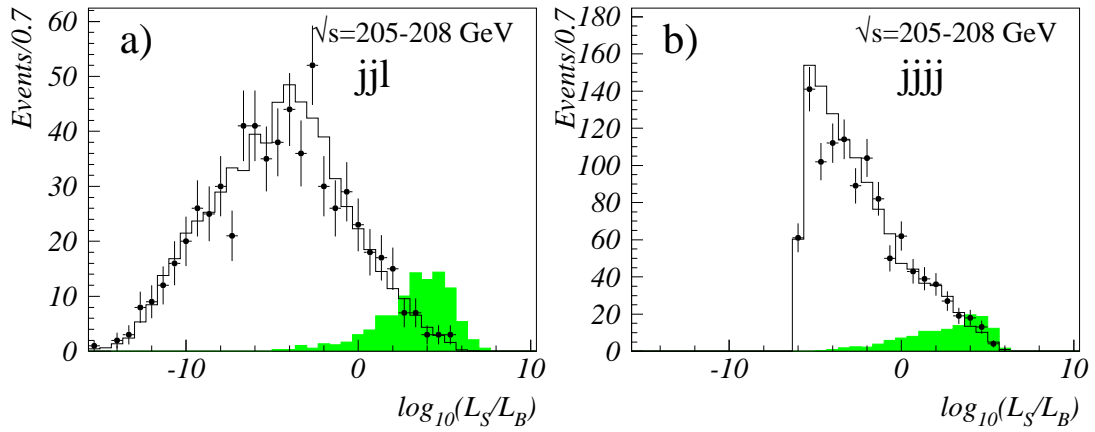


Figure 6: $\ell^*\ell^*$ search: discriminant variables in the (a) semileptonic and (b) fully hadronic channels. The dots are the data and the white histograms show the SM background expectation. The shaded histograms are the expected distributions for a $m_{L^*}=100$ GeV/ c^2 signal at $\sqrt{s} = 206$ GeV, using an arbitrary normalization.

DELPHI

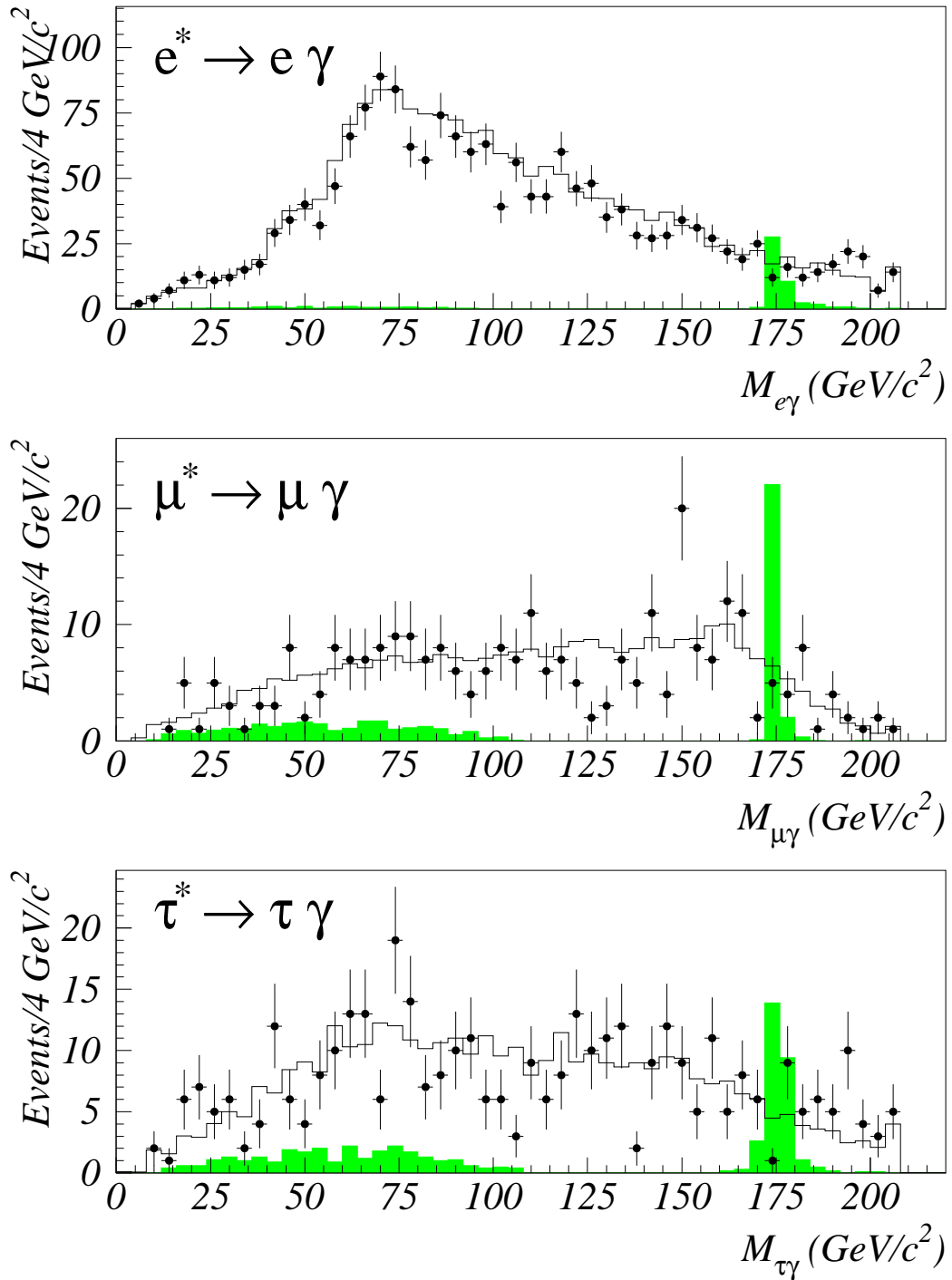


Figure 7: Lepton-photon invariant masses for the selected candidates in the $\ell^* \rightarrow \ell \gamma$ channels. Events selected in all relevant final-state topologies at all centre-of-mass energies were added. For events from the $ll\gamma$ final-state topology the two possible $\ell\gamma$ combinations are shown. The dots show the data and the white histograms show the expected SM background. The shaded histograms show the expected signal distributions at $\sqrt{s} = 206$ GeV with $m_{\ell^*} = 175$ GeV/c², using an arbitrary normalization.

DELPHI

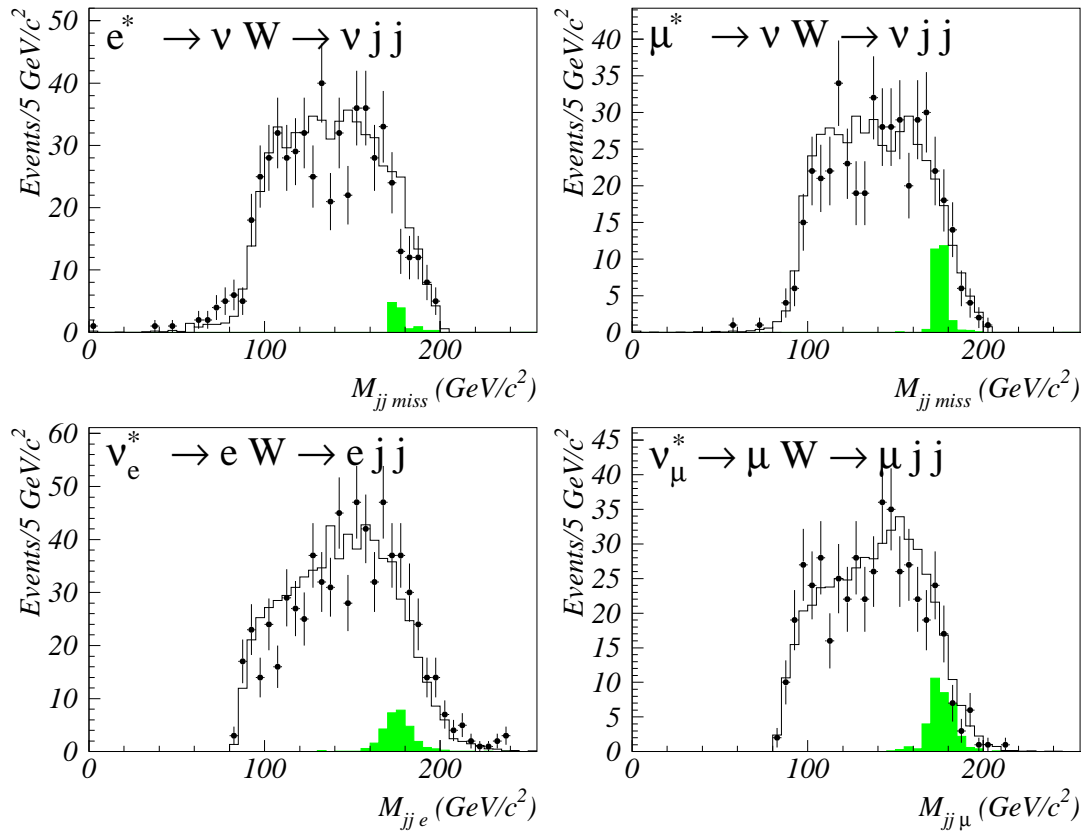


Figure 8: Invariant mass distributions for the selected candidates in the $\ell^* \rightarrow \nu W$ (top) and $\nu^* \rightarrow \ell W$ (bottom) channels. Events selected in the $jj\ell$ topology at all centre-of-mass energies were added. The dots show the data and the white histograms show the expected SM background. The shaded histograms show the expected signal distributions at $\sqrt{s} = 206$ GeV with $m_{L^*} = 175$ GeV/c^2 , using an arbitrary normalization.

DELPHI

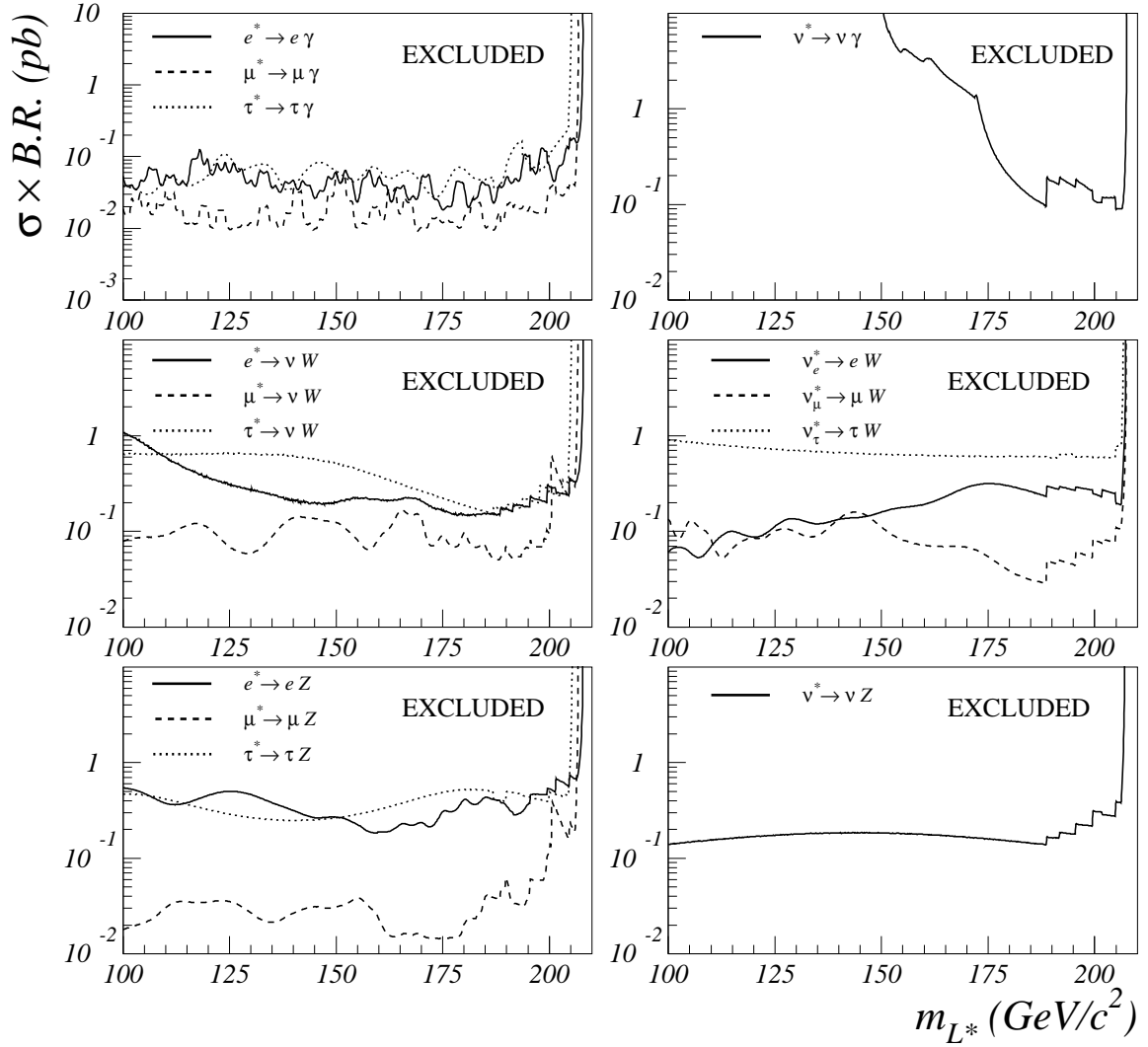


Figure 9: Results on the single production of charged and neutral excited leptons. The lines show the upper limits at 95% CL on $\sigma \times \text{BR}$ as a function of the particle mass, for each lepton flavour and decay mode.

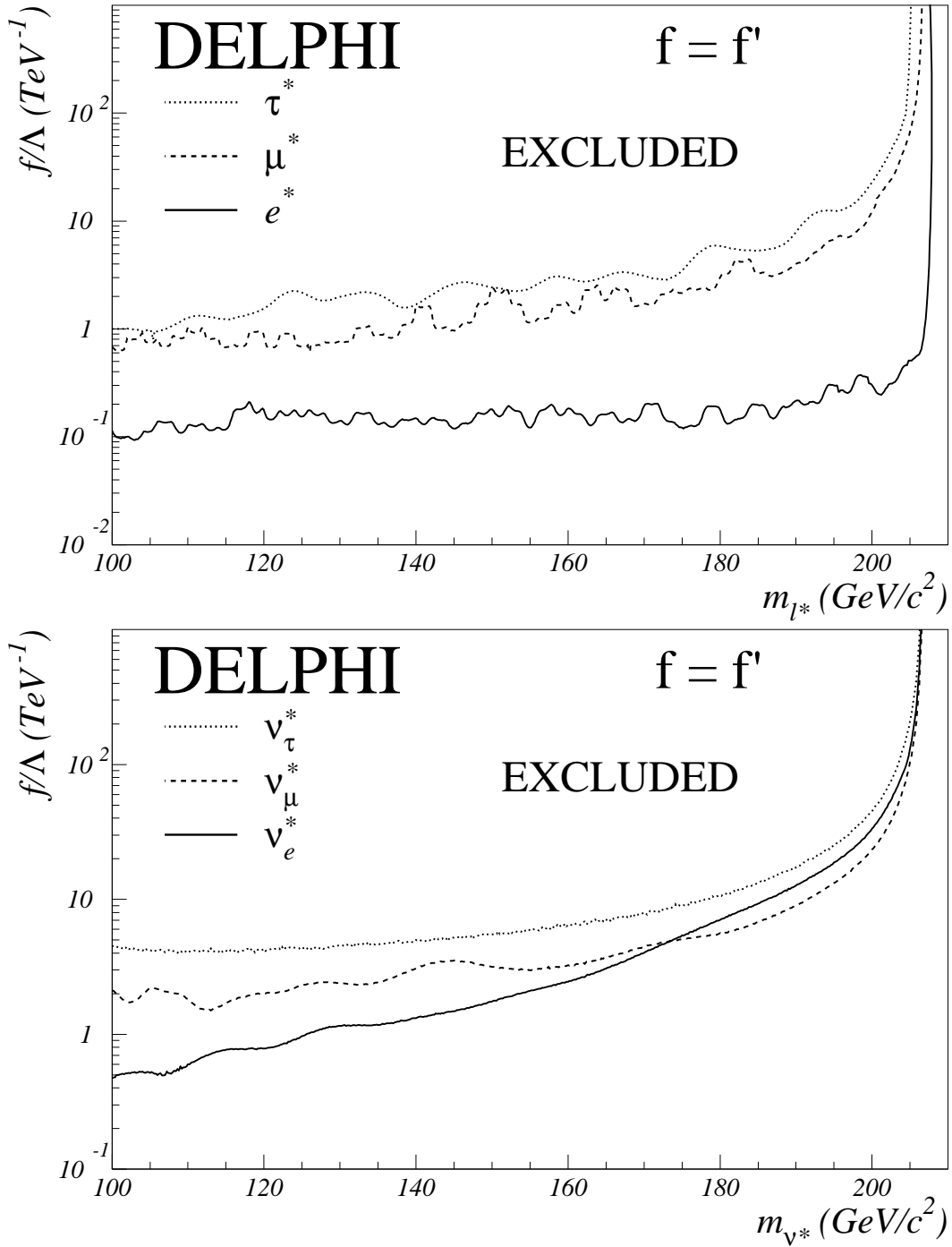


Figure 10: Results on single production of excited charged (upper plot) and neutral (lower plot) leptons assuming $f = f'$. The lines show the upper limits at 95% CL on f/Λ as a function of the excited lepton mass.

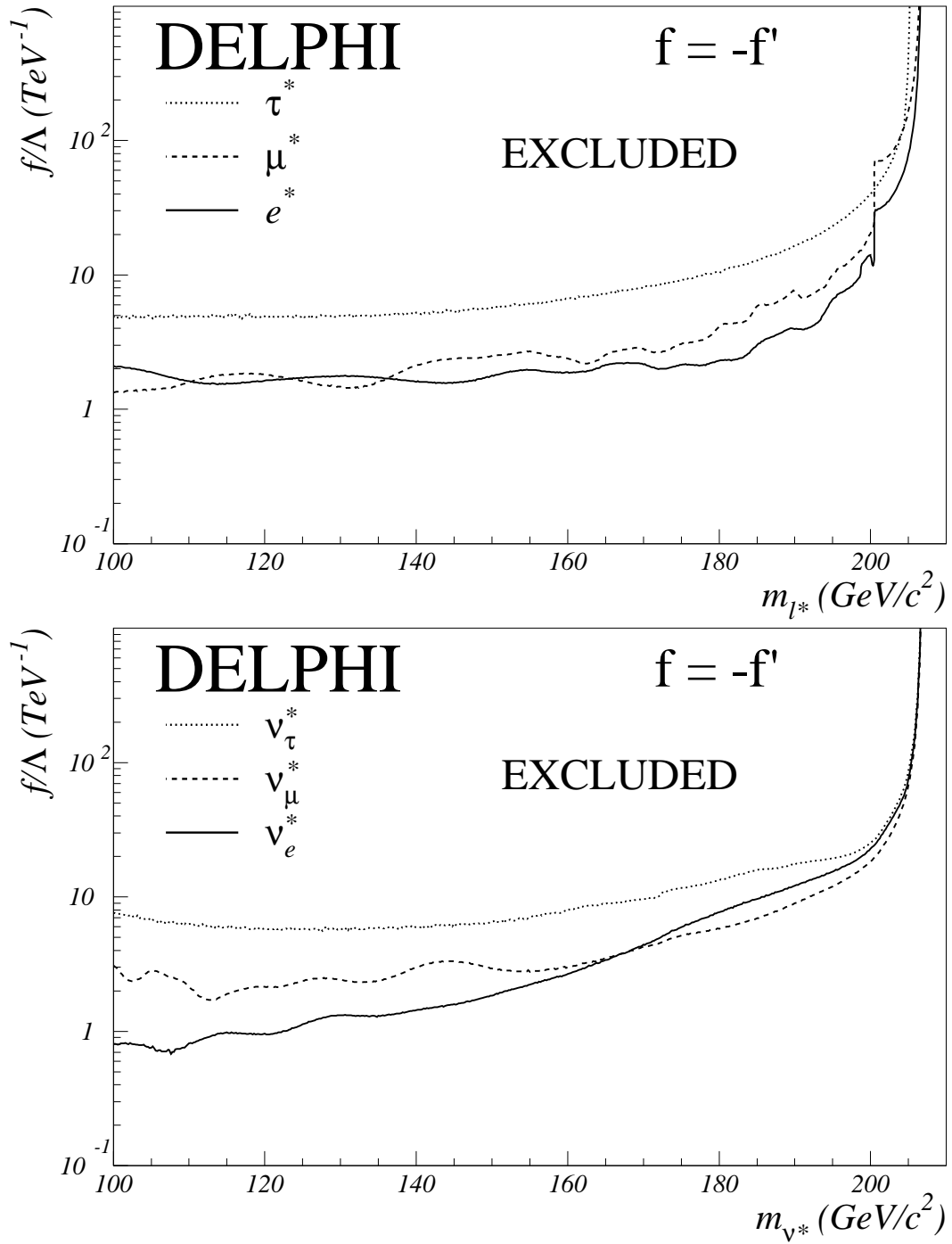


Figure 11: As figure 10, but for $f = -f'$.

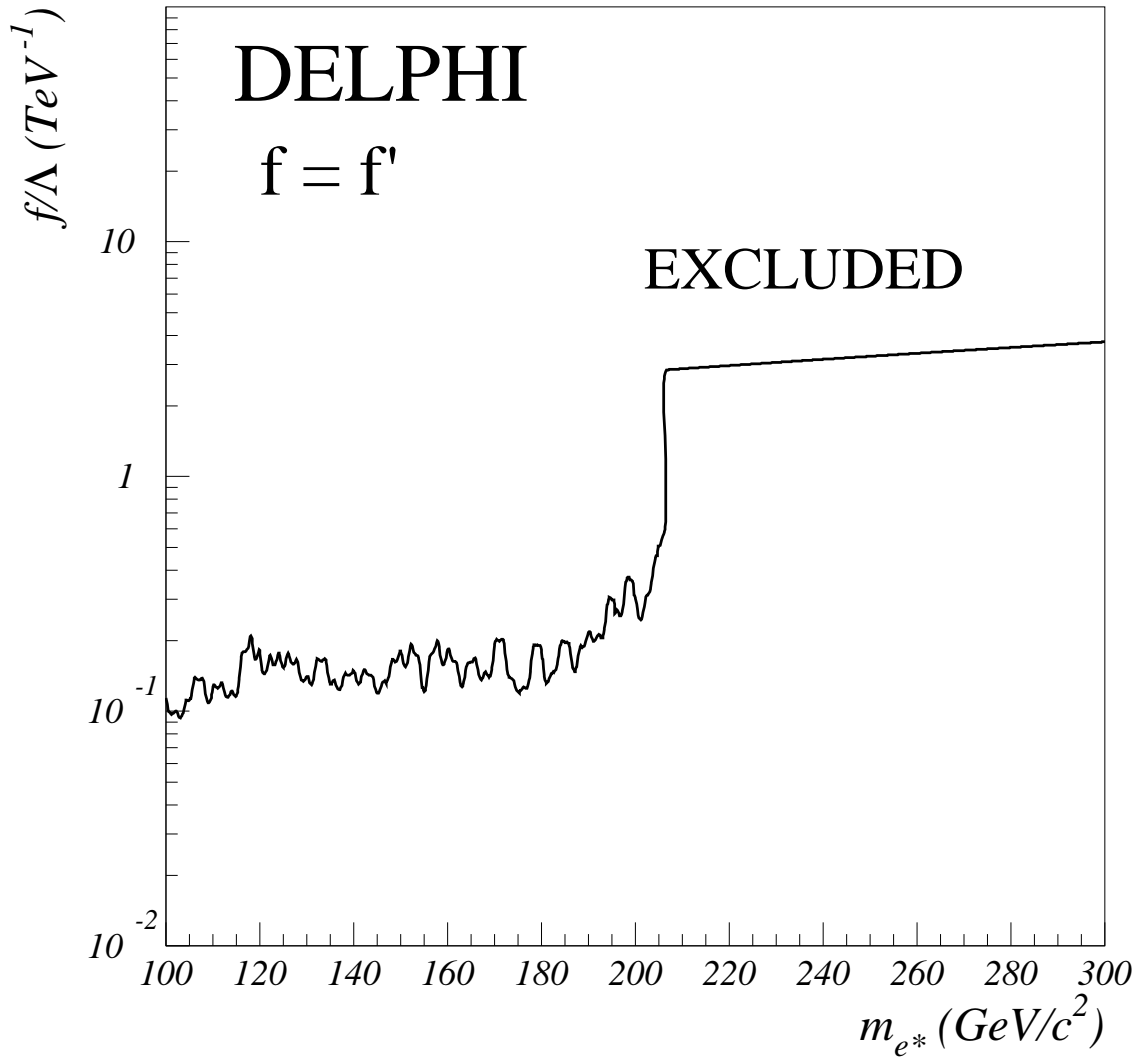


Figure 12: Combined limit on excited electron production for $f = f'$ from direct and indirect searches. The line shows the upper limit at 95% CL on f/Λ . Up to the kinematic limit the result is dominated by the direct search for single production. For masses above the kinematic limit the result stems from the indirect search of excited electron contribution to the process $e^+e^- \rightarrow \gamma\gamma$ as described in reference [25].